Work Term Report

Ioana Craiciu

May 1, 2013

Contents

List of Figures

List of Tables

1 Introduction

This report was prepared in April 2013 to summarize the work done during my four month co-op term at TRINAT. The work focuses on measuring and improving nuclear polarization of potassium for the TRINAT beta decay experiment using fluorescence curves. All of the work included in this report, except where specifically mentioned, was done with the stable isotope potassium-41.

Section 2.1 outlines Stokes parameter formalism currently used to find the degree of circular polarization of the light, S_3, points out some assumptions made by this method, and gives an expression for S_3 without those assumptions.

Section 2.2 gives the results of a test done to determine the dependence of S_3 on temperature due to the temperature sensitivity of the liquid crystal variable retarder.

Section 3 describes the fluorescence curve acquisition system that was set up during my co-op term. This includes hardware setup, trap control codes, and the typical fluorescence curves obtained. It also includes information on the errors of the fluorescence curves, which are considered to be too high. This is a problem yet to be resolved.

Section 4 describes how fluorescence curves can be used to optimize trap conditions through parameter sweeps. Fluorescence sweeps of the currents for the perpendicular field trim coils are shown, and the ideal current values derived from these are given, with the cyclotron main magnet being either on or off.

Section 5 contains the model used to find the energy levels involved in optically pumping the potassium-41 atoms to their polarized state. This includes the Hamiltonian of the system and the analytic solution given by the Breit-Rabi equation.

Section 6 describes the optical pumping setup. In particular it describes how the optical pumping and repumping frequencies are obtained. It also presents the results of tests done in the hopes of minimizing the detuning of the lasers from atomic resonances, and also to determine which of the two states of the system corresponds to σ^+ and which to σ^- light. The tests were inconclusive in both cases.

Section 7 describes how fluorescence curves were used to find coherent population trapping (CPT). This includes the CPT acquisition setup, several CPT frequency sweeps which identified the CPT frequencies of the system and the trap's magnetic field, and an unsuccessful attempt to use CPT to do parameter sweeps.

Section 8 contains some additional tests done during my co-op term. This includes measurements of the optical pumping beam power and of how the phototube background from the optical pumping beam changes with beam diameter.

Thank You

I am very thankful for the opportunity to work with TRINAT this term. It has been an incredible learning experience. Thank you in particular to John Behr for spending so much of your time teaching me about everything.

2 Circular Polarization

2.1 S3, Stokes Parameters and Mueller Matrices

Most of the derivations in this section are taken from the journal article "Polarization and the Stokes Parameters." [1] A beam of light can be described as a group of photons. If all the photons are in a coherent state, the beam is said to be polarized, and it can be described by a wavefunction. If we take the z direction to be the direction of propagation, we can describe any coherent state of photons by the wavefunction

$$\Psi = E_x e^{i(\omega t + \delta_1)} \hat{x} + E_y e^{i(\omega t + \delta_2)} \hat{y} \tag{1}$$

Density matrix formalism allows this same wavefunction to be expressed another way. A density matrix for a system which can be described as a coherent superposition of two orthogonal states has the form

$$\rho = \left[\begin{array}{cc} a_1 a_1^* & a_1 a_2^* \\ a_2 a_1^* & a_2 a_2^* \end{array} \right] \tag{2}$$

where a_1 and a_2 are the amplitudes of the two orthogonal wavefunctions. In the case of the polarized beam

$$a_1 = E_x e^{i(\omega t + \delta_1)}$$
$$a_2 = E_y e^{i(\omega t + \delta_2)} \tag{3}$$

The diagonal elements of the density matrix are called populations, because they describe the expectation value for the number of photons in each one of the orthogonal states. They are usually normalized so that $Tr(\rho) = 1$. The off diagonal elements are called coherences, and they describe the relative phase between the two states, which is constant in time.

If the photons are not coherent, the beam of light is called unpolarized. An unpolarized beam cannot be described by a wavefunction, but it can be described by a density matrix. Here also, the diagonal elements give the expectation value of number of photons in each state. These numbers are equal for completely unpolarized light (if they were not equal, the light would be have to be somewhat polarized in one direction). Because the photons are in different states, there is no constant relative phase, and the off diagonal elements are zero. Normalizing so that $Tr(\rho) = 1$, unpolarized light is described by the density matrix

$$\rho = \left[\begin{array}{cc} \frac{1}{2} & 0 \\ 0 & \frac{1}{2} \end{array} \right] \tag{4}$$

Light that is polarized to an arbitrary degree can be described as an incoherent addition of a polarized beam and a completely unpolarized one. Defining the degree of polarization P as the fraction of the beam that is in a coherent state, any beam of light can then be described by the following density matrix, where the factor of $\frac{1}{2}$ is to preserve the normalization

$$\rho = P \begin{bmatrix} a_1 a_1^* & a_1 a_2^* \\ a_2 a_1^* & a_2 a_2^* \end{bmatrix} + \frac{1}{2}(1 - P) \begin{bmatrix} 1 & 0 \\ 0 & 1 \end{bmatrix} = \begin{bmatrix} \rho_{11} & \rho_{12} \\ \rho_{21} & \rho_{22} \end{bmatrix} \tag{5}$$

Stokes parameters are another way of representing the information contained in the density matrix of a beam of light. Stokes parameters are used more frequently than density matrices to describe beams because they all correspond to observables, whereas the off-diagonal terms in the density matrix do not. They are often represented as a four vector, and their relationship to the density matrix elements are as follows

$$I = \begin{bmatrix} S_0 \\ S_1 \\ S_2 \\ S_3 \end{bmatrix} = \begin{bmatrix} \rho_{11} + \rho_{22} \\ \rho_{11} - \rho_{22} \\ \rho_{21} + \rho_{12} \\ i\rho_{21} - i\rho_{12} \end{bmatrix} \tag{6}$$

The observables are as follows:

- S_0 corresponds to the total intensity of the beam, usually normalized to 1.

- S_1 corresponds to the degree of plane polarization with respect to $\hat{x}$ versus $\hat{y}$

- S_2 corresponds to the degree of plane polarization with respect to two axes at $45°$ to $\hat{x}$ and $\hat{y}$

- S_3 corresponds to the degree of circular polarization

These observables can found using the following tests:

- S_0 is the total measured intensity of the beam, usually normalized to 1 so the other parameters give degrees of one kind of polarization.

- S_1 can be measured by placing a polarizer, which I will call the analyzing polarizer, in the path of the beam parallel to $\hat{x}$ and measuring the resulting intensity I_x, then doing the same with a polarizer parallel to $\hat{y}$ to obtain I_y, then using the formula

$$S_1 = \frac{S_1}{S_0} = \frac{I_x - I_y}{I_x + I_y} \tag{7}$$

- S_2 can be measured by the same method as S_1 with the polarizer $45°$ to $\hat{x}$ and $\hat{y}$.

- Measuring S_3 requires the use of a quarter wave plate in addition to the polarizer in order to convert circularly polarized light to plane polarized light before passing it through the polarizer.

For a polarized beam of light, the Stokes parameters obey the equation

$$S_0^2 = S_1^2 + S_2^2 + S_3^2 \tag{8}$$

This can be verified by looking at the relationship between the Stokes parameters and the density matrix elements in Equation 6 and the definition of the density matrix elements in Equation 5, setting $P = 1$. If $P \neq 1$, then the Stokes parameters obtained experimentally as described above do not obey the equality in Equation 8.

However, a beam of unpolarized light can be described by adding two Stokes vectors, one unpolarized and one polarized, analogous to Equation 5

$$I_{real} = I_{Polarized} + I_{Unpolarized} = P \begin{bmatrix} 1 \\ S_1 \\ S_2 \\ S_3 \end{bmatrix} + (1-P) \begin{bmatrix} 1 \\ 0 \\ 0 \\ 0 \end{bmatrix} = \begin{bmatrix} 1 \\ PS_1 \\ PS_2 \\ PS_3 \end{bmatrix} \tag{9}$$

Here the Stokes parameters S_1, S_2, and S_3 do obey Equation 8, but they do not correspond to the observables described above. Rather, it is PS_1, PS_2 and PS_3 that correspond to the observables.

For characterizing the circular polarization of the optical pumping beam, S_3 is found indirectly by using the relationship between the Stokes parameters (Eq. 8). This is the method used to calculate S_3 in Section 2.2. A polarizer is rotated until the maximum intensity is is observed. This is taken to be the intensity I_x. The polarizer is rotated again until the minimum intensity is observed, this is taken to be I_y, and the two are used in Equation 7 to find S_1.

In the most general case, polarized light is elliptically polarized, meaning that, over time, the vector sum of the two components of the wavefunction trace an ellipse perpendicular to the $\hat{z}$ direction. Because $\hat{x}$ and $\hat{y}$ are chosen along the directions of maximum and minimum polarized intensity, the beam is symmetrically polarized at $45°$ from either axis. Those perpendicular polarized intensities will be equal and S_2 will be 0. We can equivalently define $S_{lin}^2 = S_1^2 + S_2^2$, and use Equation 7 to find S_{lin} without making assumptions about the directions of I_{max} and I_{min}. This is the method used by M. Groves in his co-op report[2].

To find the degree of circular polarization, Equation 8 is solved for S_3 with $S_2 = 0$, giving

$$S_3 = \frac{S_3}{S_0} = \sqrt{1 - S_1^2} \tag{10}$$

Here, the assumption that $P = 1$ is being made, since the S_3 obtained from Equation 8 is equal to the degree of circular polarization only if P=1. If $P \neq 1$, the degree of circular polarization is PS_3, as seen in Equation 9. Also, the assumption is being made that the observed S_1 obeys Equation 8, which also implicitly assumes that P=1.

This method thus makes the assumption that the light reaching the analyzing polarizer is perfectly polarized. That is not to say it makes assumptions about how it is polarized (circular, plane or elliptical polarization), but only that all the photons can be described by one wavefunction, which corresponds to the polarization parameter P being 1. Another assumption being made is that the analyzing polarizer is a perfect polarizer, which means it is 100% transparent to light parallel to it's polarizing axis, and 100% opaque to perpendicular light.

To determine theoretically the effect of these assumptions on calculated values of S_3, we can use the Stokes four vector and matrix representations of optical elements encountered by the beam. Since the Stokes four vector contains all the information needed to describe the polarization of a beam of light, it can be used to mathematically represent the beam. An optical element, such as a polarizer, a quarter wave, a half wave plate, a variable retarder, etc. takes one Stokes vector and converts it to another. These elements can therefore be represented by 4×4 matrices, called Mueller matrices. The element acting on the beam is equivalent to the Mueller matrix premultiplying the Stokes vector.

The Stokes vector for a beam is found by filling out the Stokes parameters. For example, light that is perfectly right handed circularly polarized (nb. right handed circular polarization can mean either σ^+ or σ^-, depending on the convention used) and has total intensity equal to 1 will be represented by the Stokes vector

$$I_{circular} = \begin{bmatrix} 1 \\ 0 \\ 0 \\ 1 \end{bmatrix} \tag{11}$$

Light that is perfectly elliptically polarized with maximum plane polarized intensity along the $\hat{x}$ direction, with total intensity 1 will be represented by

$$I_{elliptical} = \begin{bmatrix} 1 \\ S_1 \\ 0 \\ S_3 \end{bmatrix} \tag{12}$$

or if it is not perfectly polarized, but has a degree of polarization P, it will be described by

$$I_{real} = P \begin{bmatrix} 1 \\ S_1 \\ 0 \\ S_3 \end{bmatrix} + (1 - P) \begin{bmatrix} 1 \\ 0 \\ 0 \\ 0 \end{bmatrix} = \begin{bmatrix} 1 \\ PS_1 \\ 0 \\ PS_3 \end{bmatrix} \tag{13}$$

The Mueller matrices of various optical components are easily found in literature.

9

A perfect linear polarizer in the $\hat{x}$ direction is represented by

$$M_{perfect} = \frac{1}{2} \begin{bmatrix} 1 & 1 & 0 & 0 \\ 1 & 1 & 0 & 0 \\ 0 & 0 & 0 & 0 \\ 0 & 0 & 0 & 0 \end{bmatrix} \tag{14}$$

While a partial linear polarizer along the $\hat{x}$ or $\hat{y}$ direction is represented by [3]

$$M_{real} = \frac{1}{2} \begin{bmatrix} P_x^2 + P_y^2 & P_x^2 - P_y^2 & 0 & 0 \\ P_x^2 - P_y^2 & P_x^2 + P_y^2 & 0 & 0 \\ 0 & 0 & 2P_x P_y & 0 \\ 0 & 0 & 0 & 2P_x P_y \end{bmatrix} \tag{15}$$

where P_x and P_y are transmission factors between 0 and 1, defined so that $E_x' = P_x E_x$ where E_x' is the field amplitude in the $\hat{x}$ direction after the polarizer. The analogous relationship holds for the $\hat{y}$ direction.

Let's say the analyzing polarizer used to find S_1 has transmission factors $P_\parallel$ and $P_\perp$ along its direction of polarization and the perpendicular direction, respectively. When finding I_x, $P_x = P_\parallel$ and $P_y = P_\perp$, and vice versa when finding I_y so that

$$M_{I_x} = \frac{1}{2} \begin{bmatrix} P_\parallel^2 + P_\perp^2 & P_\parallel^2 - P_\perp^2 & 0 & 0 \\ P_\parallel^2 - P_\perp^2 & P_\parallel^2 + P_\perp^2 & 0 & 0 \\ 0 & 0 & 2P_\parallel P_\perp & 0 \\ 0 & 0 & 0 & 2P_\parallel P_\perp \end{bmatrix} \tag{16}$$

$$M_{I_y} = \frac{1}{2} \begin{bmatrix} P_\perp^2 + P_\parallel^2 & P_\perp^2 - P_\parallel^2 & 0 & 0 \\ P_\perp^2 - P_\parallel^2 & P_\perp^2 + P_\parallel^2 & 0 & 0 \\ 0 & 0 & 2P_\perp P_\parallel & 0 \\ 0 & 0 & 0 & 2P_\perp P_\parallel \end{bmatrix} \tag{17}$$

Then I_x is equal to the first element of $M_{I_x} \times I_{real}$, and I_y is equal to the first element of $M_{I_y} \times I_{real}$. Solving for S_1 in terms of I_x and I_y gives

$$S_1 = \frac{(I_x - I_y)}{(I_x + I_y)} \frac{(P_\parallel^2 + P_\perp^2)}{P(P_\parallel^2 - P_\perp^2)} \tag{18}$$

As mentioned, if $P \neq 1$, the degree of circular polarization (which I'll call $S_{3\,real}$) is equal to PS_3, so, using Equation 10

$$S_{3\,real} = P\sqrt{1 - S_1^2} = \sqrt{P^2 - \left[\frac{(I_x - I_y)}{(I_x + I_y)} \frac{(P_\parallel^2 + P_\perp^2)}{(P_\parallel^2 - P_\perp^2)} \right]^2} \tag{19}$$

10

This value depends on the degree of polarization of light, P, and the parallel and perpendicular transmission coefficients of the analyzing polarizer, $P_\parallel$ and $P_\perp$. The degree of polarization of the optical pumping light is currently being assumed to be 1. Given the coherent nature of the photon source and the use of a very good polarizer on the optical arm (ColorPol VIS700 BC4), the light is expected to be very well polarized, but the exact value of P is unknown. It may also be that P must equal exactly 1, since the light all comes from a coherent source. I did not find out what P should be for the optical pumping system, even in theory.

The value of P after the polarizer in the optical arm (see Figure 1) could be found by placing the analyzing polarizer and photodiode past the optical arm polarizer and rotating the analyzing polarizer to find $I_{max} = I_x$ and $I_{min} = I_y$. Assuming the light at that point is composed of linearly polarized light and unpolarized light (as opposed to elliptically polarized and unpolarized light), we can say $S_1 = S_0 = 1$, and solving for P in Equation 18 gives

$$P = \frac{(I_x - I_y)}{(I_x + I_y)} \frac{(P_\parallel^2 + P_\perp^2)}{(P_\parallel^2 - P_\perp^2)} \tag{20}$$

I am not sure about the validity of the last assumption.

2.2 Effect of Temperature on S3

In the radioactive runs in December 2012, it was found that the MOT coils were heating up, which was affecting the functioning of the plastic scintillator detectors. To counteract this, an air conditioning unit was set up to cool the MOT chamber from the outside via flexible ducts that were attached to the chamber. The air conditioning unit was positioned close to the upward going optical arm which circularly polarizes the optical pumping beam and directs it into the chamber.

Figure 1 shows a schematic of the optical arms for optical pumping. In both arms, light comes in linearly polarized from the optical fiber. The $\lambda/2$ plate is adjusted to minimize the amount of light in the photodiode, and therefore maximize the amount of light transmitted through the polarizing beamsplitter. The polarizer (ColorPol VIS700 BC4) is lined up with the polarization axis that is transmitted by the polarizing beamsplitter. Light exiting the polarizer is therefore linearly polarized and maximized in intensity. The liquid crystal variable retarder (Meadowlark) is alternately a $\lambda/2$ plate or a 0λ plate. It is controlled externally by the code that runs the MOT and optical pumping cycles. The light after the liquid crystal variable retarder (LCVR) is linearly polarized, either along the polarization axis of the polarizer or perpendicular to it, depending on the LCVR's state. The light then goes through the Semrock filter (LL01-780-30-0), which transmits the optical pumping light (but reflects MOT light), and through the $\lambda/4$ plate. The $\lambda/4$ plate converts linearly polarized light to circularly polarized light, either σ^+ or σ^-, depending on the state of the LCVR.
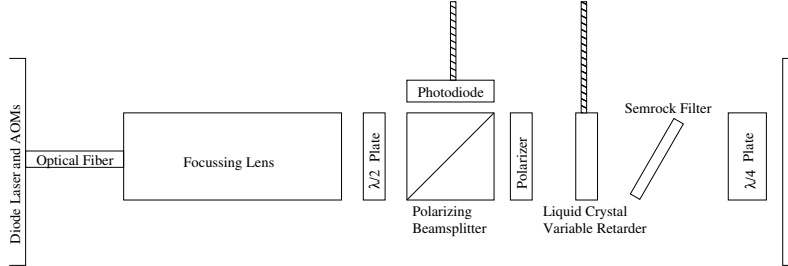
Figure 1: Schematic of optical arms for upward and downward optical pumping light

While all these elements were exposed to cold temperatures, it is assumed that only the liquid crystal variable retarders would be significantly affected. Unlike most optics, LCVRs contains birefringent nematic liquid crystal. The retardance depends on the orientation of the liquid crystal, which is controlled by an applied voltage. Changing the ambient temperature results in a viscosity change in the liquid crystal, which in turn and changes its response to voltage. Meadowlark cites a 0.2% to 0.4% decrease in retardance per increase in °C [4]. The $\lambda/4$ plate needs to be aligned with, or at 90° from, the axis of polarization to create circularly polarized light. A small deviation in retardance in the LCVR results

in misalignment and the $\lambda/4$ plate will produce elliptically instead of circularly polarized light.

The relationship between LCVR temperature and S_3 in the optical pumping system was investigated. The method outlined in Section 2.1 of finding S_3 (assuming perfectly polarized light and a perfect analyzing polarizer) was used. For the downward going beams, the analyzing polarizer (ColorPol VIS700 BC4) was placed between the $\lambda/4$ plate and the chamber, and a photodiode (Newport 818-SL) was placed on the other side of the chamber, mounted on the optical arm of the upward going beam. For the upward going beam, both the analyzing polarizer and the photodiode were placed on the arm of the downward going beam, facing the chamber. $I_x=I_{max}$ and $I_y=I_{min}$ were measured by reading the output signal of the photodiode on an oscilloscope. The temperature was measured at the base of either optical arm, on a steel nut fastened to the chamber. The air conditioner was turned on and measurements were taken over a few hours to obtain S_3 for a range of temperatures. During the January tests the AC MOT coils and their cooling system were not turned on, except for the last upward going beam test at 6.4 $^\circ C$, which was done 1.5 hours after the coils were turned on.

For the test in April, the AC MOT coils and their cooling system, as well as the nuclear acquisition hardware were turned on for several hours before the test, to simulate better the conditions during the radioactives run in December 2012. The position of the polarizer was also different for the April test: it was placed between the $\lambda/4$ plate and the chamber on the upward going beam arm. The results from all tests are shown in Figure 2.
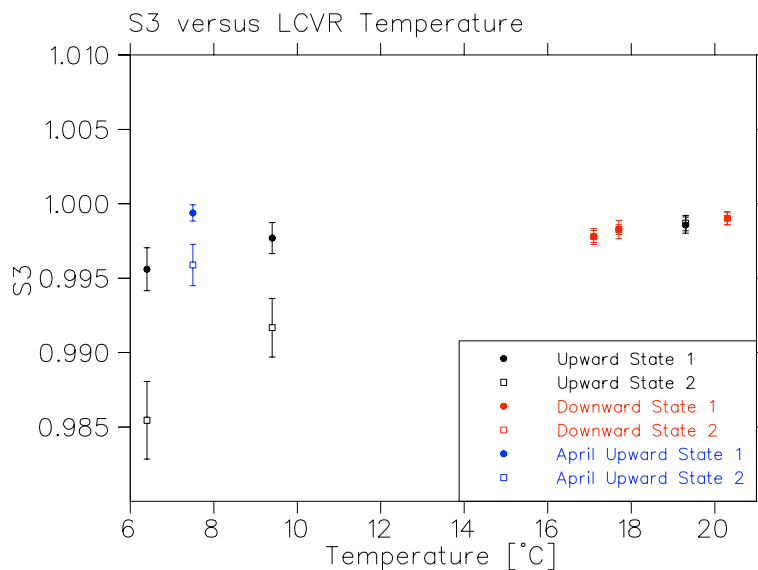
Figure 2: S_3 versus LCVR Temperature

Figure 2 shows that the downward beam optical arm did not significantly cool. This

13

is because it is far away the air conditioning unit, on the other side of the chamber. The upward beam optical arm, however, cooled down to 6 $°C$. The temperature at the LCVR was not as low, measuring 12.4 $°C$ when the base measured 7.5 $°C$ (April). The ambient room temperature near the diode was was 20.4 $°C$, in January, 21.0 $°C$ in April, and 19.4 $°C$ in December. The S_3 value was found to decrease down to 0.985 in the January test, but the April test only showed a decrease to 0.9958 only for a similar temperature. State 2 for the upward beam, and State 1 for the downward beam were more affected by a decrease in temperature. Both these states correspond to the lower voltage on their respective LCVRs, indicating that the LCVR is more sensitive to temperature in that state.

There is a large difference in the polarization measurements for the upward going beam between January and April. This could be explained by the different temperature conditions, caused by the AC MOT coils being on for different periods of time before the test. It could also be caused by the different placement of the polarizer relative to the chamber (after it in January, before it in April). If it is the former, the April measurement is likely more reliable because the conditions were closer to those in December (AC MOT and nuclear acquisition hardware on for several hours before). If it is the latter, the April measurement is again likely to be more reliable, because placing the polarizer right after the quarter wave plate should give a more accurate representation of the circular polarization of light entering the chamber than placing the polarizer after the chamber, at which point the beam has been transmitted through two viewports and reflected twice.

3   Fluorescence Curves

During optical pumping, potassium atoms (either ^{37}K or ^{41}K) are optically pumped from the $S_{\frac{1}{2}}$ state to the $P_{\frac{1}{2}}$ state using circularly polarized light. This results in the atoms reaching a stretched state, either $S_{\frac{1}{2}}, F = 2, m_F = +2$ if σ^+ light is used, or $S_{\frac{1}{2}}, F = 2, m_F = -2$ if σ^- light is used. The m_F and σ directions are taken to be positive in the direction of the dominant field, which is created on axis with the optical pumping beams by the main MOT coils. These atomic states correspond to states of nuclear polarization, since the ^{37}K or ^{41}K nuclei will necessarily be in a polarized state, $I = \frac{3}{2}, m_I = +\frac{3}{2}$, or $I = \frac{3}{2}, m_I = -\frac{3}{2}$, respectively. Optical pumping is accomplished by simultaneously pumping the atoms with two circularly polarized laser beams, one resonant with the $S_{\frac{1}{2}}, F = 2 \rightarrow P_{\frac{1}{2}}, F = 2$ transition, called the pumping beam, and one resonant with the $S_{\frac{1}{2}}, F = 1 \rightarrow P_{\frac{1}{2}}, F = 2$ transition, called the repumping beam. As the atoms absorb the light and decay randomly, the population of atoms exhibits a random walk towards the stretched state. Throughout this process, the atoms are fluorescing as they decay to the ground state. When the atoms are in the stretched states, they can no longer absorb the circularly polarized optical pumping light (having reached their maximum m_F state), so they stop fluorescing. Analyzing the fluorescence of the atoms versus time during optical pumping can therefore give information on the polarization state of the nuclei. The limit of fluorescence for long optical pumping times, which ideally goes to zero, gives information about the fraction of unpolarized nuclei, while the overall shape of the curve can give information on factors affecting the optical pumping process such as perpendicular fields.

3.1   Fluorescence Curve Acquisition Setup

One of the goals of this project was to create a system that would produce fluorescence curves quickly, with the possibility of viewing them online. For this reason, a system of 11 scalers (digital pulse counters), was devised to count fluorescence photons in 11 bins, and produce an 11 point fluorescence vs. optical pumping time curve.

Figure 3 shows the fluorescence curve acquisition setup. Fluorescent photons are counted by a phototube (Hamamatsu R636-10) set at 30° to the optical pumping beam axis. There is an angle dependent filter (Semrock LL01-780-25) in front of the phototube to block trap light, but allow optical pumping and fluorescence light. The signal from the phototube is amplified by a Timing Filer Amplifier (Ortec 454), then passed to a discriminator (LeCroy 621BL) that converts analog photon signals into digital signals 100 ns in width. The signal from the discriminator is then passed into the clock inputs of all the scalers. The scalers are on two boards within the computer. Scalers 1-5 are on the first System Timing Controller chip (Am9513), and scalers 6-10 are on a the second similar chip, both on the CIO-CTR10HD board. Scaler 11 is counter 1 on a CMOS Programmable Intervel Timer (Intersil 82C54) on the CIO-AS08-AOH board. All scalers are set to a mode where they can be reset on command, then count pulses from their clock input continuously only

when gated, then read out on command. For scalers 1-10 this is Mode E and for scaler 11 this is Mode 0. Information on the scalers and their boards is available in their manuals.
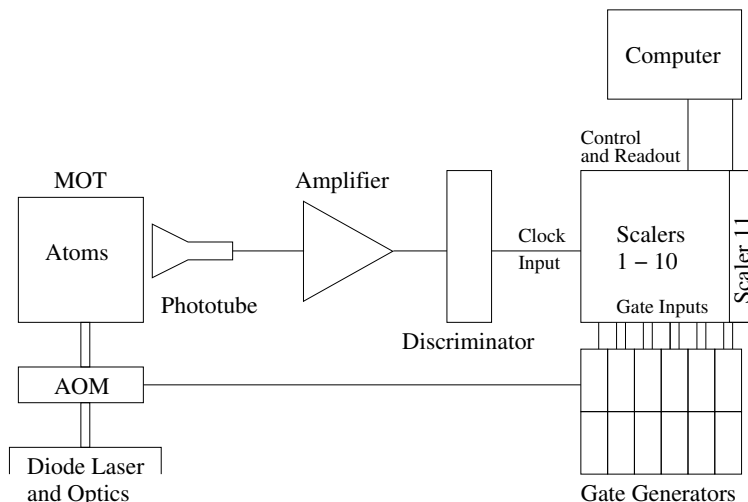
Figure 3: Schematic of fluorescence curve acquisition setup

The scalers all receive the same clock input, but they count at different times of the optical pumping cycle because they are gated at different times. This is accomplished by using 12 gate generators (6 LeCroy 222 Dual Gate Generators). Each gate generator accepts an start signal as a trigger to start outputting a gate of variable width, adjusted by a tuning a potentiometer. At the end of the gate it also sends a pulse on its delay output. Optical pumping light is turned on and off in the MOT by an acousto-optic modulator (AOM-12, Isomet 1206 C). The AOM, and therefore the optical pumping light, is on for 1.8 ms, then off for 3 ms, and this is repeated 100 times for every iteration of the trap control code. The signal controlling this AOM is connected to the first gate generator. This is set to a 1 μs gate width, which is the amount of time it takes the AOM to switch states before any fluorescence is detected, so it is not necessary to count during this time. Its delay output is connected to the start input of the next gate generator. This next generator has 1 μs gate width. Its gate output goes to the first scaler gate input, and its delay output goes to the start input of the next gate generator. The rest of the gate generators are similarly linked. In total, 12 gate delay generators gate 11 scalers one after another, with the first not providing a gate to any scaler. The gate width are usually set as shown in Table 1. They increase almost exponentially to account for the fact that fluorescence decreases exponentially, so larger counting bins are needed at longer times. The count rate in each scaler can be found by dividing the count in one AC MOT/optical pumping cycle by the scaler gate width and by 100.

The trap control code adds more atoms to the MOT and traps them, then resets the

Table 1: Scaler gate widths

Scaler	1	2	3	4	5	6	7	8	9	10	11
Gate Width (μs)	1	1	2	5	10	20	50	110	300	500	750

scalers and loads them (prepares scalers 1-10 to count, scaler 11 loads itself on the first ungated clock pulse). The hardware setup in Figure 3 then ensures that when optical pumping occurs, each scaler will be gated for the time specified in Table 1 $\times 100$ times. Once optical pumping finishes, the code saves the count value in each scaler and reads it out. The code is set up to do 16 repeats of this. The set of 16 is called (or can be called) a sweep, because it is possible in every code to sweep across 16 values of a parameter in the 16 repeats. There are several versions of the trap control code which include the scalers, described in Table 3, each being slightly different in what it what it does and/or what it displays online. All versions of the code print out the same information in the Kxxx.OUT file, with the 4th column being the repeat number n, the 5th column being *ntoggle*, discussed next, and columns 6 - 16 being the photon counts for the 11 scalers in the order they are gated.

In most versions of the code, sweeps alternate between "fluorescence" and "background" for one polarization state, then alternate again between "fluorescence" and "background" for the other polarization state. These sweeps are identified, both in the code and the output file by the *ntoggle* value, as can be seen in Table 2. These four sweeps forms what can be called a "supersweep."

Table 2: Meaning of *ntoggle*

ntoggle	Sweep Type
0	state 1 fluorescence
1	state 1 background
2	state 2 fluorescence
3	state 2 background

For the background sweeps, the idea is to have no atoms in the trap, so that any light detected by the phototube is known to be from the background source (ie. the optical pumping beams). This light background plus the phototube's random firing background will have a constant value which can then be subtracted from the "fluorescence" sweeps to obtain the true fluorescence value. The method for obtaining a "background" sweep is to kick out any atoms at the end of the previous sweep by shifting the trap light to the blue, turning off the constant magnetic field, and not pushing over any atoms from the

first trap for the duration of the sweep. It was observed, by looking at the phototube's signal on an oscilloscope when there were no atoms in the trap, that in the first 5 μs of optical pumping the background is not flat, but has a small bump, increasing to around 5% of its otherwise constant value. This is likely due to transient effects in the AOM after it is turned on. Another issue with the background is the fluctuation of laser power. The "background" is taken approximately 8 seconds after the beginning of its corresponding "fluorescence" sweep, and during this time the laser power can change, resulting in fewer or more background photons than were present in the "fluorescence" sweep.

Table 3: Trap Control Codes Using Scalers

Code	Description
d7sccal2	*Calibration.* Used to calibrate the gate widths after tuning them manually. Follows *ntoggle*, but online averaged display adds instead of subtracting "background" runs. "Now" plot shows number of counts. To be used with the trap background or a source of known frequency as the clock input.
d7scsw2	*Fluorescence curves.* Used to generate fluorescence curves. Follows *ntoggle*. Online averaged plots update every other sweep and show "fluorescence" minus "background" for State 1 (called $-$) and State 2 (called $+$) separately. "Now" plot shows latest sweep.
d7scswp2	*Fluorescence parameter sweep.* Used to optimize nuclear polarization by sweeping a parameter. Follows *ntoggle*. Requires connecting DAC 8 to the input of parameter control system, and inputing upper and lower limits of DAC 8 in the param.dat file. Parameter swept from lower to upper limit in 16 steps. Online averaged plots show the 16 tail to peak ratios (Eq. 21) for State 1 ($-$) and State 2 ($+$) separately. "Now" plot shows latest sweep.
d7sccpt	*Coherent population trapping.* Used to detect coherent population trapping. Requires setup outlined in Section 7 including changing the gate widths. Follows *ntoggle*. Averaged plots show count rates for first 6 scalers and last 5 scalers separately. "Now" plot shows latest sweep.
d7cptswp	*Coherent population trapping parameter sweep.* Used to optimize nuclear polarization by sweeping a parameter. No background subtraction: skips *ntoggle* = 1 and 3. Requires use of DAC 8 as in d7scswp2. Online averaged plots show the 16 CPT ratios (Eq. 22) for State 1 ($-$) and State 2 ($+$) separately. "Now" plot shows latest sweep.

$$Tail\,to\,Peak^* = \frac{SC10 - SC10B + SC11 - SC11B}{SC1 - SC1B + SC2 - SC2B} \qquad (21)$$

$$CPT\ Ratio^* = \frac{SC8 - SC11 + SC9 - SC11B}{SC1 - SC11 + SC2 - SC11 + SC3 - SC11} \qquad (22)$$

$^*SCX(B) = average\ count\ rate\ in\ scaler\ X\ during\ ``fluorescence"\ (during\ ``background")$

3.2   Typical Fluorescence Curves and Errors

A typical fluorescence curve obtained with this system, using d7scsw2, is shown in Figure 4, on a semi-log plot. The fluorescence can be seen to exponentially decay to level almost equal to the background. The errors in this graph are root-mean-square errors (RMS) for the data. For this curve, the number of supersweeps was 9, but the first supersweep was excluded due to transient effects observed in the first two sweeps. This is observed for every sweep. So each count rate data point corresponds to $8 \times 16 = 128$ measurements. The RMS errors are significantly larger than the counting errors predicted for the scalers, as seen in Figure 5. This points to a systematic cause for the errors.

One systematic is a change in the number of atoms in the trap from one sweep to another. This is very likely to occur, and the effect it would have on the fluorescence curve is to scale the entire curve by a different gain factor for every sweep, and in fact for every optical pumping cycle. Averaging over several optical pumping cycles with different gain factors will lead to a high RMS error.

Another systematic is the change in laser power as previously mentioned. During the S_3 versus temperature measurements, observing both the optical arm photodiode (shown in Figure 1) and the analyzing diode over time showed that the laser power did drift, on the time scale of several minutes. The backgrounds are due mostly to the optical pumping light, and it is likely their errors are a result of its power drift.

It was observed that the peak of the fluorescence curve (with the rest of the curve scaling in a similar way), was consistently lower for the first 4 optical pumping cycles of every sweep. This is shown in Figure 6, which was obtained with d7scpsw2 without sweeping over any parameter. In the figure, the backgrounds are subtracted, error is added in quadrature, and the fits are power law fits, described in Section 4. It is possible that during these four optical pumping cycles there are fewer atoms in the trap. Excluding the first four cycles decreases the RMS error in the fluorescence data significantly, as seen in Figure 7. It is interesting to note that excluding the first four cycles also decreases the background RMS error a small amount. This is indicative that it is not only the number of atoms that is different in the first four sweeps, but also the laser power. This could be due to a long lived transient effect of the AOM.

It should also be noted that the background curves are not completely flat. It was initially thought that this is due to poor precision in the gate widths of the scalers, leading to errors in determining count rates from counts. However, the gate widths for Figure 4 have been calibrated using a 200 kHz square wave generator, and the non-uniformity has

not disappeared. Specifically, scaler 11 seems to have a higher count rate than the rest. Scaler 2 is also somewhat high, and this is possibly due to the transient "bump" that was observed in optical pumping light power.

Overall, the RMS errors indicate that there are systematic errors associated with the fluorescence curve acquisition system. Several have been identified above. Some have been corrected for: excluding the first supersweep, excluding the first 4 of 16 cycles of each sweep, and calibrating the scaler gate width. The varying number of atoms in the trap and the drift of the laser power over time have not yet been corrected for. Correcting for the varying number of atoms in the trap would require knowing the number of atoms, which can be obtained from the CCD camera image of the atoms. Correcting for the laser power drift would require knowing the laser power, which can be accomplished by sampling a portion of the laser beam. This could prove to be challenging depending on where in the optical pumping optics the drift is occurring.
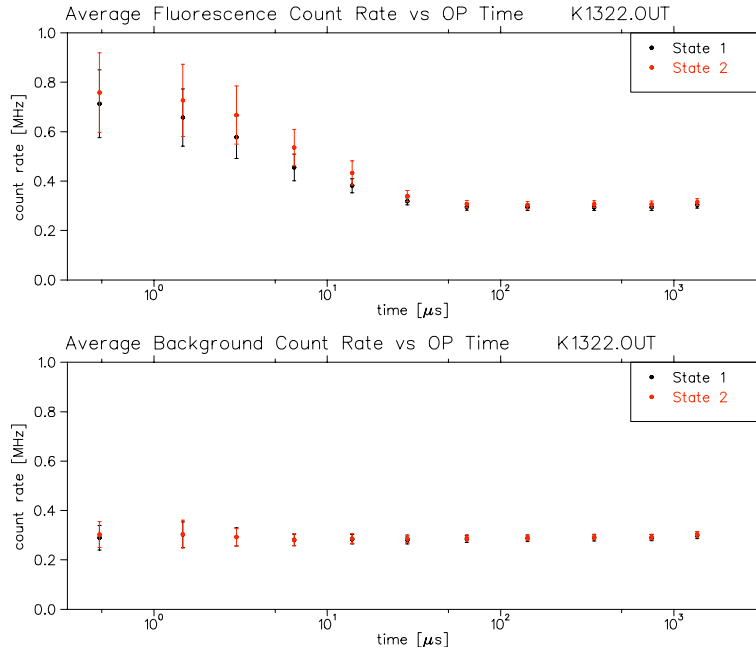
Figure 4: Typical fluorescence curve
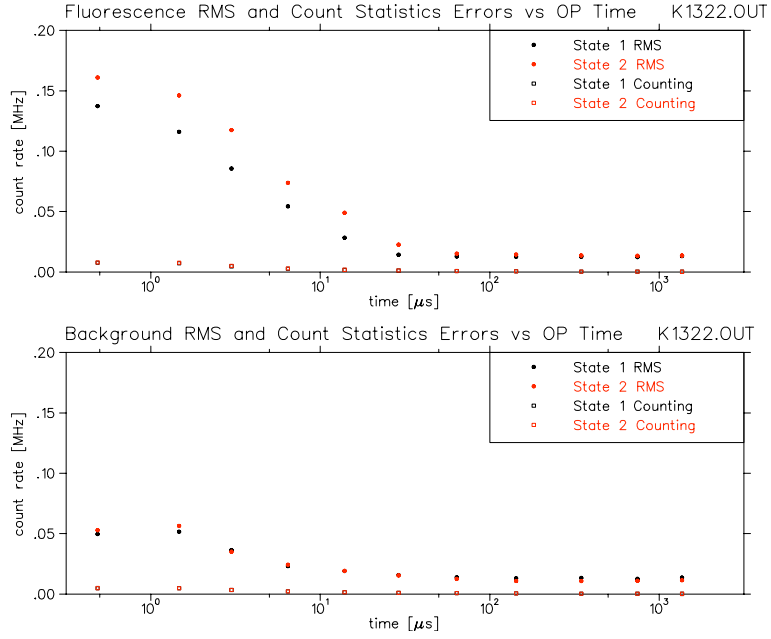
Figure 5: RMS and counting errors of typical fluorescence curve
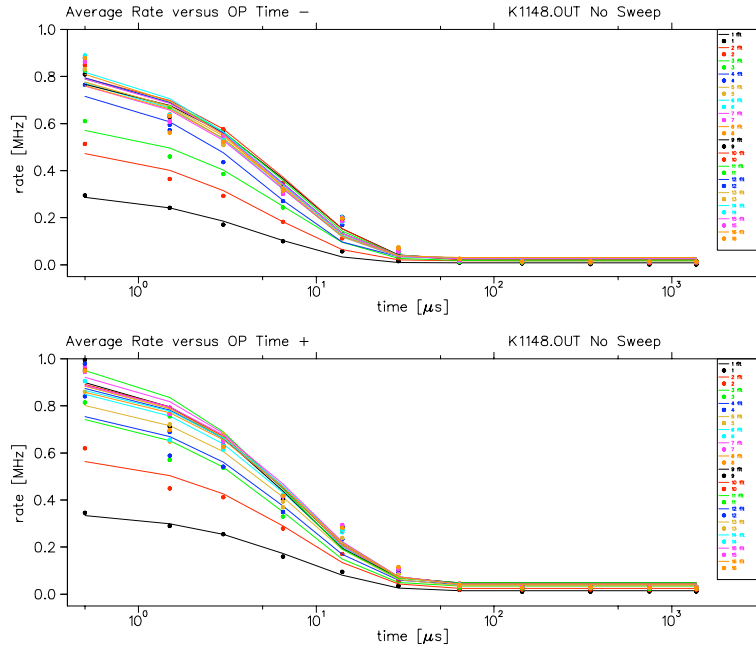
Figure 6: Fluorescence curve sweep without changing a parameter, with power law fits

21
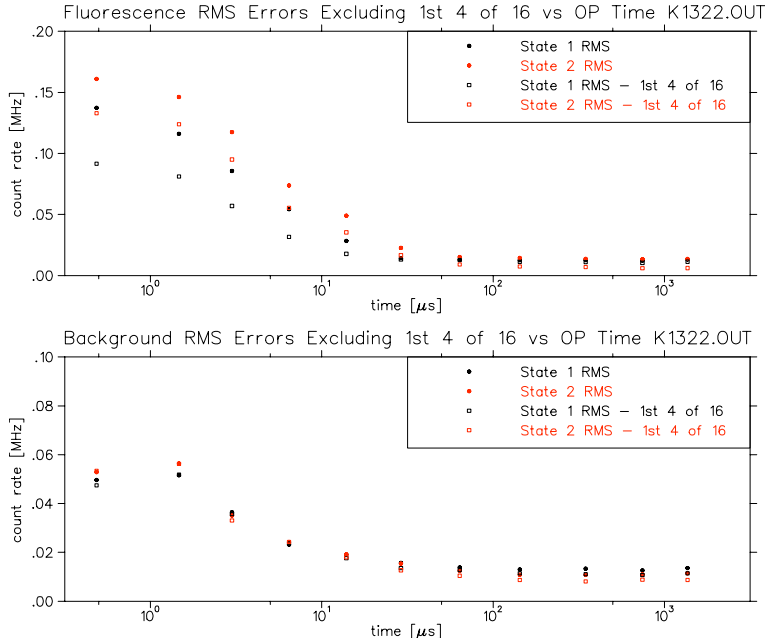
Figure 7: Fluorescence RMS errors, with and without first 4 optical pumping cycles

4 Parameter Sweeps Using Fluorescence Curves

As mentioned in Section 3, the limit of the fluorescence curve at long times — the *tail* of the curve — gives information about the number of unpolarized nuclei. This value scales with the number of atoms in the trap, which can vary. Normalizing to the number of atoms in the trap is done by dividing the tail value by the initial fluorescence value — the *peak* of the curve — which should only depend on the number of atoms in the trap. Sweeping over a parameter, such as a perpendicular trim field, with d7scpsw2 and finding the minimum tail to peak ratio will therefore give the value of that parameter which maximizes nuclear polarization. The equation used to display tail to peak online is shown in Equation 21, but this is not the only way of expressing the tail to peak ratio.

4.1 Power Fits to the Fluorescence Curves

Due to the unresolved issues with RMS errors, tail to peak ratios found using Equation 21 had unrealistically large error bars. To get around this, the fluorescence curves were fit with following power law equation:

$$count\,rate = a \times b^{time} + c \tag{23}$$

In the most basic optical pumping model with 4 levels, the probability of atoms being

22

in an unpolarized state goes as

$$P = \left(\frac{2}{3}\right)^N \tag{24}$$

where N is the number of atomic transitions. Since fluorescence count rate is a measure of the atoms in unpolarized states, is not surprising that a power law fits the fluorescence data quite well. However, $b \neq \frac{2}{3}$, because potassium atoms are not 4 state systems and b also includes a factor of $1^{\frac{N}{time}}$.

The fluorescence curves for each step of the parameter sweep were fit in Physica with a power law (after averaging over all supersweeps and subtracting the backgrounds from the fluorescence data) and $\frac{c}{a}$ was taken as the tail to peak ratio. The fit was weighted by $1/\sigma^2$, where σ is the RMS error of the data. The $E2$ errors of the fit parameters were combined in quadrature to obtain the errors of the tail to peak ratio. This gave reasonable errors for the tail to peak ratios. Figure 8 shows an example of a weighted power law fit to a set of data (with no sweep), the derived tail to peak ratio, and its errors. The errors in the data set are RMS errors. Because the errors are smaller at later times, the power law underestimates the peak of the curve. This was observed consistently. One other thing to note is that the power laws were not binned in fitting the data, but assumed that the binned scaler counts were data points on a curve, which leads to some error.
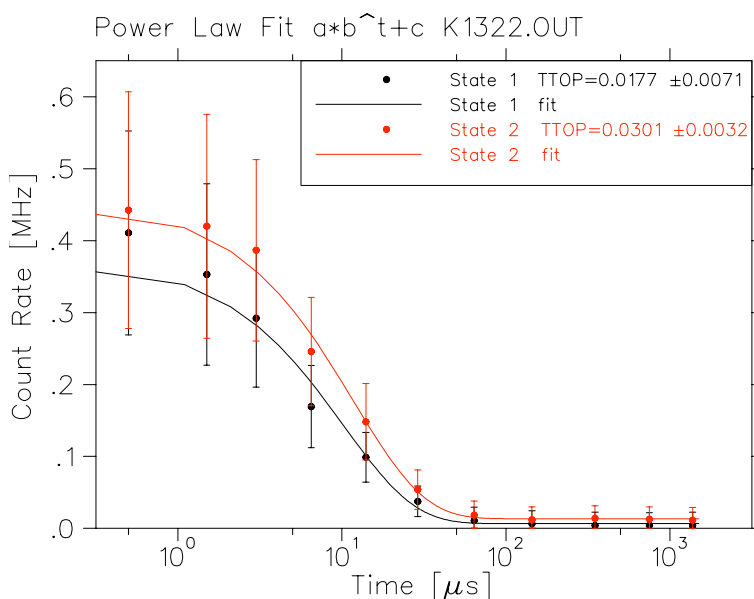
Figure 8: Typical weighted power law fit of a fluorescence curve

4.2 Minimizing Trim Fields: Cyclotron Off

For optical pumping to occur, the direction of propagation of light and the direction of the magnetic field in the region occupied by the atoms must be the same. Any perpendicular components of the field will lead to mixing of the states with different m_F. To eliminate perpendicular fields in the trap, which exist predominantly due to the earth's magnetic field and the main cyclotron magnet, electromagnet coils are wound around the chamber and the frame. The desired field is straight up and down. One set of coils, called the B_{Z2} coils, is wound around the frame, creating a field roughly along the East-West axis. The other set, the B_{X2} coils, is wound around the chamber, creating a field roughly along the North-South axis. Both sets of coils are referred to as "trim" coils.

In early March, tail to peak sweeps were carried as described in the previous section, with the current in the coils as the sweep parameter. At that time, the cyclotron magnet was not turned on. The results of the sweep are shown in Figures 9 and 10. The graph for B_{Z2} is a composites of more than one sweep. Not shown is a repeated sweep of the B_{X2} sweep done in the opposite direction, that was consistent with the one shown. The graphs have well defined minima, found by fitting a quadratic function to the curve. The fit was of the form $a(x-b)^2 + c$, where the "min" value in the graphs is equal to b, and its error is the E2 error. The quadratic function seems to fit the data well, particularly in Figure 9. A minimum tail to peak indicates maximum nuclear polarization, so the optimal settings for the trim coils appear to be $I = -0.47$ A for B_{X2} and $I = 0.19$ A for B_{Z2}. It is interesting to note that the location of the minima differ slightly between State 1 and State 2 in both sets of coils.
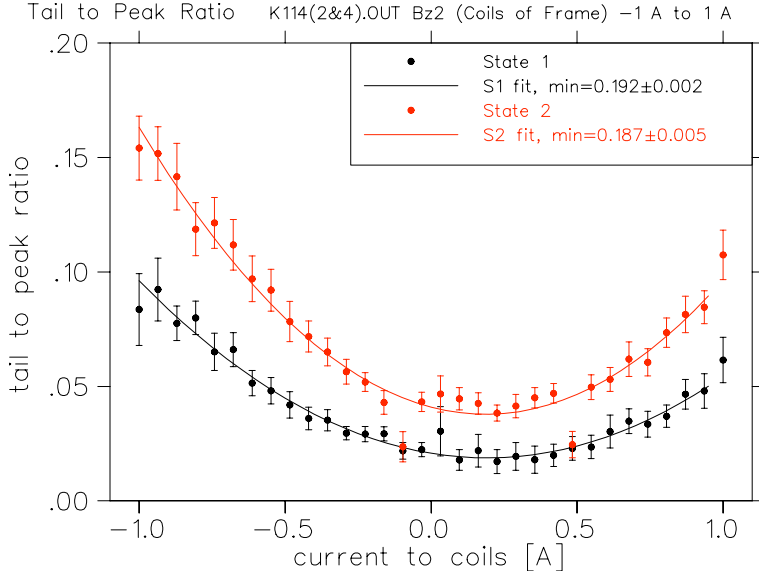
Figure 9: Trim coils sweep: on frame, cyclotron off

24
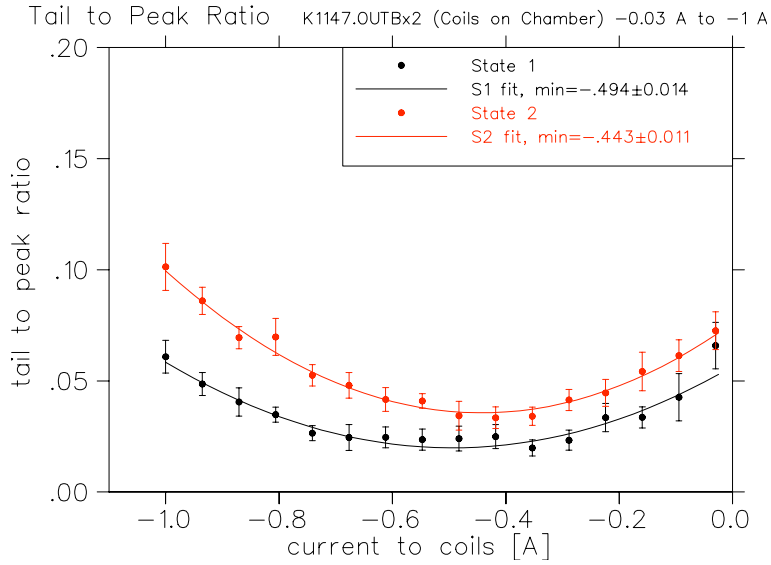
Figure 10: Trim coils sweep: on chamber, cyclotron off

4.3 Minimizing Trim Fields: Cyclotron On

In late March, after the main cyclotron magnet was turned on, the trim coil sweeps were re-done. The results are shown in Figures 11 and 12. The ideal current for B_{X2} changed slightly to $I = -0.54\ A$.

For the State 1 B_{Z2} sweep, the fit shown is an unweighted fit as the error bars were too large to obtain a reasonable weighted quadratic fit that gave a result similar to that of State 2. For State 1 the errors on the ideal current shown in the graph are not realistic, but the ideal current appears to be somewhere around $I = 0.5\ A$. For State 2, the weighted fit gives an ideal current of $I = 0.62\ A$. Compared to the B_{X2} coils, this is a larger change from when the cyclotron is off, but this is expected for the East-West direction, due to the relative position of the cyclotron to the MOT. The minima are slightly different from the settings used for the December 2012 runs, which were $I_{B_{X2}} = -0.49\ A$ and $I_{B_{Z2}} = 0.82\ A$. However, it can be seen from the figures that the tail to peak ratio changes very little between $I_{B_{Z2}} = 0.5\ A$ and $0.82\ A$ and between $I_{B_{X2}} = -0.49\ A$ and $-0.54\ A$, so this difference is not a problem.

25
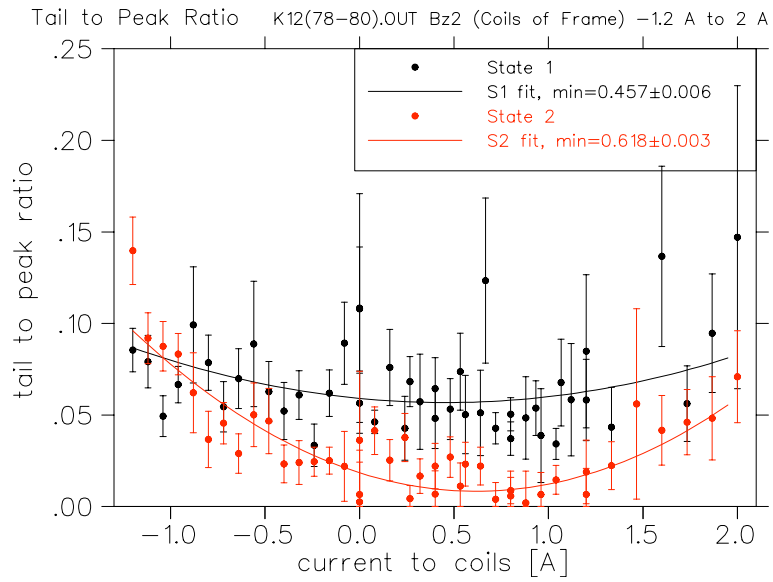
Figure 11: Trim coils sweep: on frame, cyclotron on
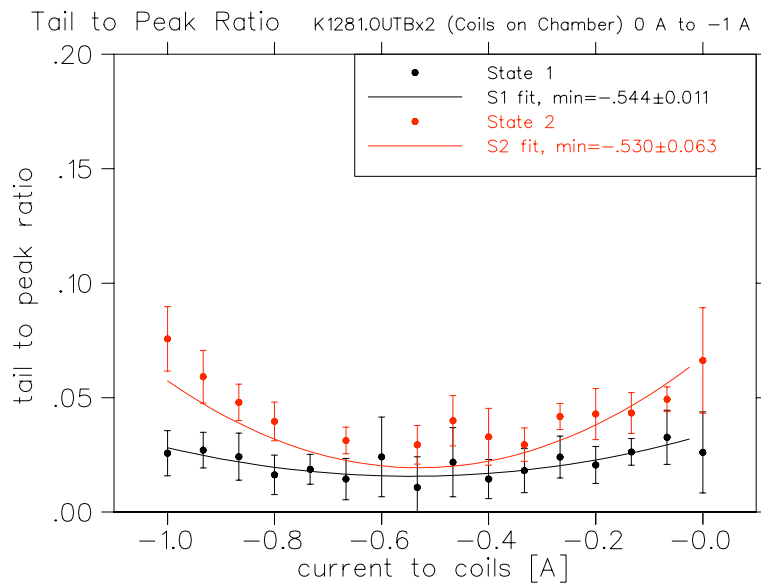
Figure 12: Trim coils sweep: on chamber, cyclotron on

26

5   Modeling The $S_{\frac{1}{2}}$ and $P_{\frac{1}{2}}$ Energy Levels

For the work done in Sections 6 and 7, it was necessary to know the energy diagram of the $S_{\frac{1}{2}}$ and $P_{\frac{1}{2}}$ states involved in optical pumping. This section is largely based on Reference [7]. This is fairly simple because potassium is an alkali atom and therefore it is hydrogen-like. Both states are in the same $n = 4$ shell, so the Coulomb interaction can be taken as constant for both. The spin-orbit interaction does not split the energy levels of the states because they have equal J. The Lamb shift does split the $S_{\frac{1}{2}}$ and $P_{\frac{1}{2}}$ states. This splitting (corresponding to the hyperfine-free D_1 transition frequency in potassium) is empirically measured to be 389286294.205(62) MHz for ^{41}K [5]. The remaining terms of the Hamiltonian for both states are the hyperfine interaction and the Zeeman interaction of the electron and nucleus with the magnetic field.

$$H = H_{Hyperfine} + H_{Zeeman-Electron} + H_{Zeeman-Nucleus} \tag{25}$$

where

$$H_{Hyperfine} = A_J \mathbf{I} \cdot \mathbf{J} \tag{26}$$

$$H_{Zeeman-Electron} = g_J \mu_B \mathbf{B} \cdot \mathbf{J} \tag{27}$$

$$H_{Zeeman-Nucleus} = -g_I \mu_N \mathbf{B} \cdot \mathbf{I} \tag{28}$$

Because both these states have total atomic angular momentum J=$\frac{1}{2}$, there is an analytic solution for the energy levels of this Hamiltonian, given by the Breit-Rabi Formula

$$E_{Fm_F} = -\frac{h\nu_{HFS}}{2(2I+1)} - g_I \mu_n B m_F \pm \frac{h\nu_{HFS}}{2}\left\{1 + \frac{4m_F x}{2I+1} + x^2\right\}^{\frac{1}{2}} \tag{29}$$

where

$$x = \frac{(g_J + g_I M_e/M_P)\mu_B B}{h\nu_{HFS}} \tag{30}$$

$$\mu_B = \frac{e\hbar}{2M_e} \tag{31}$$

$$\mu_n = \frac{e\hbar}{2M_P} \tag{32}$$

$$m_F = m_I \pm m_J = -2, -1, 0, 1, 2 \tag{33}$$

27

The eigenvalues of the system are $|F \, m_F\rangle$ states. The plus sign in Equation 29 and should be used for the F=2 states, and the minus for the F=1 states. B is the magnetic field, I is the nuclear spin, $I = \frac{3}{2}$, M_e and M_p are the electron and proton masses, h is Planck's constant, and e is the unit charge. ^{41}K specific constants are shown in Table 4.

Table 4: Breit-Rabi Formula Constants

Constant	Value
$\nu_{HFS} = 2A_J/h$	254.013870(1) MHz for $S_{\frac{1}{2}}$[6]
	$2 \times 15.245(42) MHz$ for $P_{\frac{1}{2}}$[5]
g_I	-0.000077906[6]
g_J	2.00229421(24) for $S_{\frac{1}{2}}$[6]
	2/3 for $P_{\frac{1}{2}}$[theory]

Using this equation, the energy of every $|F \, m_F\rangle$ state for both $S_{\frac{1}{2}}$ and $P_{\frac{1}{2}}$ can be found. Together with the hyperfine-free transition frequency D_1, these energy levels can be used to find all the all the atomic resonances of the potassium atom for the $S_{\frac{1}{2}} \to P_{\frac{1}{2}}$ transition. These resonances depend on the magnetic field B.

All but the stretched $|F \, m_F\rangle$ states are mixtures of the $|m_J \, m_I\rangle$ states. However, if m_F is taken to be in the direction of B, these mixtures only contain states with $m_F = m_I + m_J$. For example, $|F = 1 \, m_F = 1\rangle$ is a mixture of $|m_I = +\frac{3}{2} \, m_J = -\frac{1}{2}\rangle$ and $|m_I = +\frac{1}{2} \, m_J = +\frac{1}{2}\rangle$ and nothing else. Introducing a perpendicular B field results in each eigenstate being a mixture of more $|m_J \, m_I\rangle$ states this. This was found by diagonalizing the Hamiltonian in Equation 25 using MATLAB, and looking at the composition of the eigenvectors. The MATLAB script "BreitRabi.m" diagonalizes the Hamiltonian in Equation 25 and solves the Breit-Rabi formula, both of which give the same energy levels, and calculates detunings based on AOM frequencies (discussed in Section 6). It can be found on trcomp under /home/trinat/apr2013.

A diagram of the energy levels of $S_{\frac{1}{2}}$ and $P_{\frac{1}{2}}$ states of ^{41}K is shown in Figure 13. This includes the Zeeman splitting for a field of $B = 2.19 \, G$, found by CPT sweeps to be the magnetic field in the trap during optical pumping when the cyclotron is on (see Section 7).

Energy (MHz)

	−2	−1	0	1	2	mF

F=2 10.41 10.95 11.47 11.97 12.46
F=1
      −18.57 −19.09 −19.59   P$_{1/2}$

- -

F=2 92.18 93.75 95.29 96.81 98.32   S$_{1/2}$

389 286 294 MHz

F=1
      −157.25 −158.80 −160.32
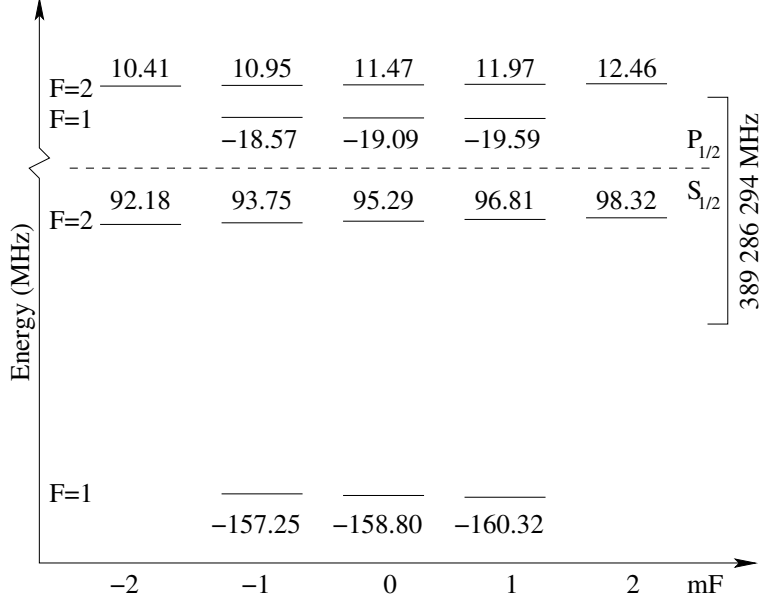
Figure 13: ^{41}K Energy levels with 2.19 G Field

6 Detunings and Distinguishing σ^+ From σ^-

6.1 Optical Pumping Setup

The optical pumping and repumping beams are supplied by a diode laser (TUI Optics DL100). Their frequencies are fixed by locking onto a saturation spectroscopy peak of ^{39}K, and offsetting that frequency using a series of AOMs and an RF generator. Figure 14 shows this setup. Light from the diode laser is passed through a beam sampler, then through a double pass AOM (Isomet 1206C), AOM-SAS in the figure. The light passes through the AOM twice, after which the beam with $\nu_{laser} - 2\nu_{AOM-12}$ is chosen and passed to the saturation spectroscopy cell, where ν_{AOM-12} is positive.

In the saturation spectroscopy cell, the beam is split into two counter-propagating beams, both of which pass through a sample of gaseous potassium atoms. At any point in time, a small fraction of the atoms have zero velocity on axis with the beams, so that they experience no doppler shift. For these atoms, when the beams are on resonance, one beam excites them, and they will be unable to absorb the opposite beam, resulting in a dip in the absorption spectrum. The resonant frequencies of the atoms can be found by sweeping over frequencies of the laser and observing dips in the absorption spectrum. This saturation spectrum of ^{39}K is shown (inverted) in Figure 15, with various transitions of ^{39}K are labelled. The frequencies on the x-axis were chosen so that resonances of ^{39}K match the identified peaks. This frequency sweep is achieved by sweeping the piezo

voltage of the diode laser. The laser frequency (offset by $-2\nu_{AOM-12}$), is locked onto the $S_{\frac{1}{2}}$, $F = 2 \rightarrow P_{\frac{1}{2}}$, $F = 1 - 2$ transition with the laser's lock-in amplifier, where $F = 1 - 2$ is the half energy level (an energy level halfway between two states that doesn't correspond to a real state) between $F = 1$ and $F = 2$. Frequencies corresponding to half energy levels show up on saturation spectroscopy peaks because they can excite certain atoms with nonzero axial velocity due to the two beams being Doppler shifted by the same amount (one to the red, one to the blue). A similar effect leads to the sideband induced peaks seen in Figure 15.

The frequency locked laser beam then goes through AOM-12 (Isomet 1206C), which gives the necessary offset to excite ^{37}K atoms (or ^{41}K atoms, with a different offset). Overall, the optical pumping frequency is given by

$$\nu_{pumping} = \nu_{laser} + \nu_{AOM-12} \tag{34}$$

where

$$\nu_{laser} = \nu_{sat\,spec} + 2\nu_{AOM-SAS} \tag{35}$$

$$\nu_{sat\,spec} = \nu_{(^{39}K\,F=2\rightarrow F=1-2)} = 389285878.631 MHz$$

$$\nu_{AOM-12} = 131.7 MHz$$

The repumping frequency is created in the same laser beam as the pumping frequency by pumping the laser diode with radio frequency. This creates RF sidebands in the laser spectrum, seen in Figure 16. The upper sideband is the one that repumps the atoms. The RF generator that usually pumps the diode is a Mini-Circuits Voltage Controlled Oscillator (ZOS-300). However, as part of the CPT setup discussed in Section 7, a second RF source (HP 8640B Signal Generator) and an RF switch (Mini-Circuits ZYSWA-2-50DR) were added. The repumping frequency is given by

$$\nu_{repumping} = \nu_{pumping} + \nu_{RF\,Generator} \tag{36}$$

The system has the possibility of changing pumping and repumping frequencies from State 1 to State 2. State 1 and State 2 correspond to two different states of the LCVR and therefore to the two different states of circular polarization (σ^+ and σ^-). Since there is a constant magnetic field parallel to the beams and the total g-factor for the ^{41}K is positive, the Zeeman effect makes $m_F \rightarrow m_F + 1$ transitions in ^{41}K have slightly higher frequencies, on average, than $m_F \rightarrow m_F - 1$ transitions. This can be seen by looking at Figure 13. Since the former transitions are allowed with σ^+ light, and the latter with σ^-, the average of the resonant frequencies for each polarization state is different. It could therefore be helpful to change the laser frequency from one state to another. This is accomplished by changing the frequency of the double pass AOM, which is controlled by the code. The RF sideband frequencies can also be changed by switching between RF sources with the RF switch, which can also be controlled by the code via the signal sent to toggle the LCVR between states.
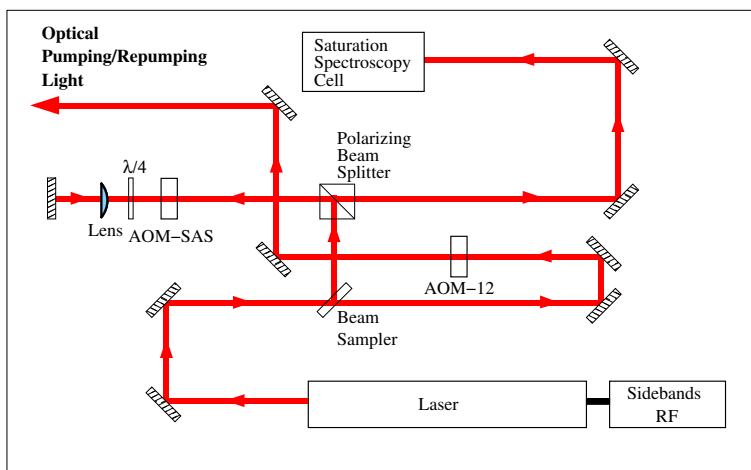
Figure 14: Optical pumping frequencies setup
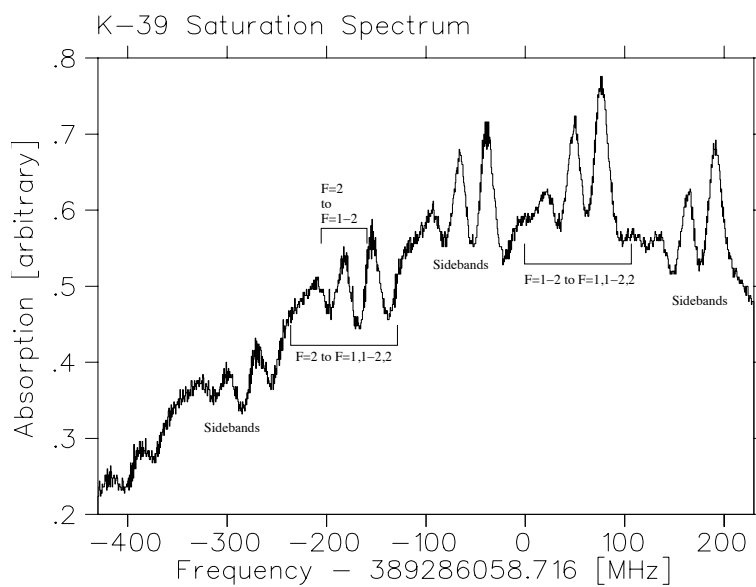
Figure 15: ^{39}K saturation spectroscopy curve
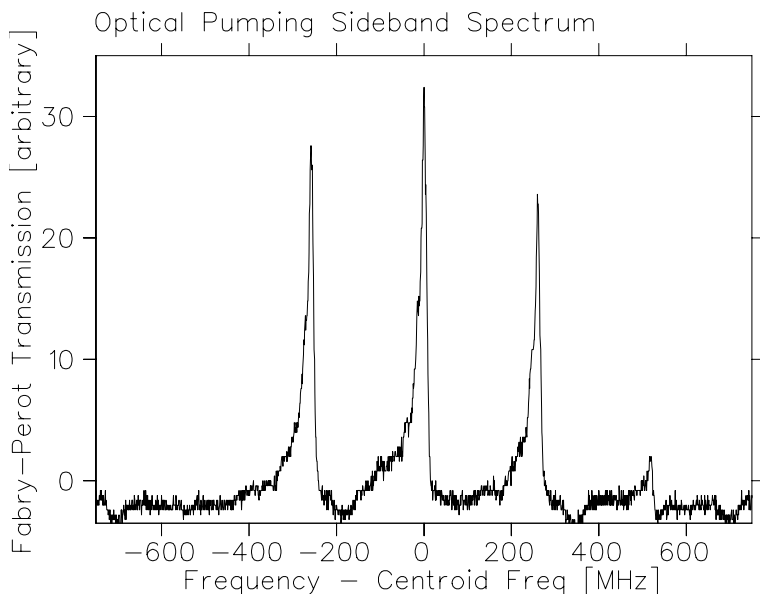
Figure 16: Pumping centroid and repumping sidebands on laser frequency spectrum

6.2 Distinguishing σ^+ from σ^-

At this time, it is unknown whether State 1 corresponds to σ^- and State 2 corresponds to σ^+, or the other way around. State 1 corresponds to certain voltages on the LCVRs (5.625 V for the upward beam, 1.858 V for the downward). State 2 corresponds to different voltages on the LCVRs (2.038 V for the upward beam, 6.34 V for the downward). Both states also have their own laser frequency, determined by frequencies of the double pass AOM and the RF sidebands. However, it is not known which LCVR voltages correspond to σ^- or σ^+, so it is not possible to optimize the optical pumping and repumping frequencies for the two states.

An attempt was made to determine which state had which polarization by changing the optical pumping and repumping frequencies and observing the resulting fluorescence curves. At the same time, an attempt to minimize the detunings in the system to improve nuclear polarization was made, where the detuning of a transition is defined as

$$Detuning = Laser\,Frequency\,for\,Transition - Atomic\,Resonance\,for\,Transition \quad (37)$$

The model in Section 5 can be used to find the atomic resonances, and the laser frequency for that transition can be found using Equations 34 to 36 given $\nu_{AOM-SAS}$ (double pass AOM) and $\nu_{RF\,Generator}$, which were the independent variables. It is impossible to make all the detunings zero, since there are seven transitions with slightly different resonances but only two laser frequencies (pumping and repumping).

Several combinations of pumping and repumping frequencies which theoretically minimized detunings in different ways were used, and the tail to peak ratios were found as described in Section 4. As can be seen in Table 5, the difference between trials with the same parameters are of the same order as differences between trials with different parameters. Since none of the tail to peak ratios were remarkably different, and here are many parameters in this problem, so it was hard to extract any information from the tail to peak values obtained. None of the other parameter combinations led to smaller tail to peak ratios for both States than the runs done "as in December." It may be possible that the tail to peak ratio cannot be further minimized. The line-widths of the atomic transitions are around 6 MHz [5]. Sine the detunings calculated for any the transitions in any of the runs in Table 5 are lower than 6 MHz, and since, as previously mentioned, only two of seven transitions can have detunings of exactly zero, it may be that there are a range of pumping and repumping frequencies that give about the same nuclear polarization.

Since the tail to peak ratios found with a power law fits did not give conclusive evidence as to which state had which polarization, the next step taken was to try to fit the curves with a model containing more physics. More specifically, by fitting the data with a model that distinguishes between polarization states, a fit assuming one polarization state might fit the data better than a fit assuming the other polarization state, and the better fit would indicate the correct polarization state. The code containing this model, written by John Behr, finds the energy levels of the atoms given the field in the trap and models the atomic transitions classically. It includes considerations for laser power, transient and permanent perpendicular fields (leading to precession of states), laser detunings, and the value and sign of S_3.

Figures 17 and 18 are two fluorescence curves fit by this model. One fit was done for each state (State 1 or State 2) of the fluorescence curves. The runs chosen were such that the laser frequencies corresponding to State 1 (of the LCVR) in one run corresponded to State 2 (of the LCVR) in the other run. For clarity, one set of frequencies was labelled A, and the other B, and the graphs are labelled accordingly. All the other parameters in the runs were the same, and all parameters entered into the model are listed in Table 6. The perpendicular field was floated by quadratic interpolation between 3 curves solved for $B_{perp} = 0, 0.025, 0.05\,G$. To find out if State 1 of the "K1322.OUT" run corresponded to σ^- or σ^+, it was fit using the parameters in Table 6 and either a negative or positive sign for S_3, giving the blue and red curves in the "State 1" section of Figure 17, respectively. The same was done for State 2 of that run, and for both states of the other run. The hope was that the σ^- would fit the State 1 data in both runs, and σ^+ would fit the State 2 data in both runs, or vice versa. However, by looking at Figures 17 and 18, it is obvious that this is not the case. Therefore, this method also was unable to identify which state corresponds to which circular polarization.

Table 5: Tail to Peak Ratio for Different Detunings

| File | Tail To Peak Ratio | | Detunings |
	State 1	State 2	
K1322.OUT	0.0177 ± 0.0071	0.0301 ± 0.0032	As in December
K1339.OUT	0.0108 ± 0.0088	0.0396 ± 0.0054	As in December
K1332.OUT	0.0245 ± 0.0079	0.0211 ± 0.0037	As in December
K1350.OUT	0.0359 ± 0.0070	0.0528 ± 0.0051	Simulates ^{37}K Optical Pumping
K1329.OUT	0.0338 ± 0.0040	0.0644 ± 0.0046	As in December, Swapped
K1334.OUT	0.0253 ± 0.0033	0.0871 ± 0.0070	Correct Isotope Shift
K1340.OUT	0.0382 ± 0.0098	0.0278 ± 0.0049	Correct Isotope Shift
K1341.OUT	0.0218 ± 0.0098	0.0206 ± 0.0056	Correct Isotope Shift
K1335.OUT	0.0348 ± 0.0057	0.0816 ± 0.0075	If State 1 is σ^+ minimizes detunings for $m_F = \pm1$ to $m_F = \pm2$
K1344.OUT	-0.0023 ± 0.0074	0.1078 ± 0.0098	If State 1 is σ^+ minimizes detunings for $m_F = \pm1$ to $m_F = \pm2$
K1338.OUT	0.0299 ± 0.0077	0.0713 ± 0.0085	If State 1 is σ^- minimizes detunings for $m_F = \pm1$ to $m_F = \pm2$
K1336.OUT	-0.0029 ± 0.0084	0.1501 ± 0.0122	If State 1 is σ^+ minimizes detunings for $m_F = \pm1$ to $m_F = \pm2$ (one SB freq. wrong)
K1337.OUT	0.0147 ± 0.0075	0.0591 ± 0.0043	If State 1 is σ^- minimizes detunings for $m_F = \pm1$ to $m_F = \pm2$ (one SB freq. wrong)
K1342.OUT	0.0299 ± 0.0066	0.0466 ± 0.0072	If State 1 is σ^+ minimizes detunings for $m_F = \pm1$ to $m_F = \pm2$ (F=2 to F=2) and $m_F = 0$ to $m_F = \pm1$ (F=1 to F=2)
K1343.OUT	0.0099 ± 0.0086	0.0395 ± 0.0051	If State 1 is σ^+ minimizes detunings for $m_F = \pm1$ to $m_F = \pm2$ (F=2 to F=2) and $m_F = 0$ to $m_F = \pm1$ (F=1 to F=2)

There is another way in which σ^- and σ^+ can be distinguished, and that is from the resulting direction of polarization of the nuclei relative to the magnetic field. This in turn which can be deduced in the radioactive runs from beta or recoil distributions. The direction of the field must also be known for this method. Looking at the beta or recoil distributions in State 1 and State 2 should answer the question of which σ corresponds to which state.

Table 6: Distinguishing σ^- and σ^+: Laser States A and B

Parameter	Value
Pumping beam power	$0.399\,mW/cm^2$
Repumping beam power	$0.1992\,mW/cm^2$
Initial value of decaying perpendicular field	$0.0165\,G$
Constant perpendicular field	Floated
S_3 value	0.9988
Detunings for Laser State A (for $B = 0$)	
$\|F = 2, m_F = 2\rangle \to \|F = 2, m_F = 2\rangle$	$-1.333\,MHz$
$\|F = 1, m_F = 2\rangle \to \|F = 2, m_F = 2\rangle$	$-0.346\,MHz$
Detunings for Laser State B (for $B = 0$)	
$\|F = 2, m_F = 2\rangle \to \|F = 2, m_F = 2\rangle$	$2.667\,MHz$
$\|F = 1, m_F = 2\rangle \to \|F = 2, m_F = 2\rangle$	$3.654\,MHz$
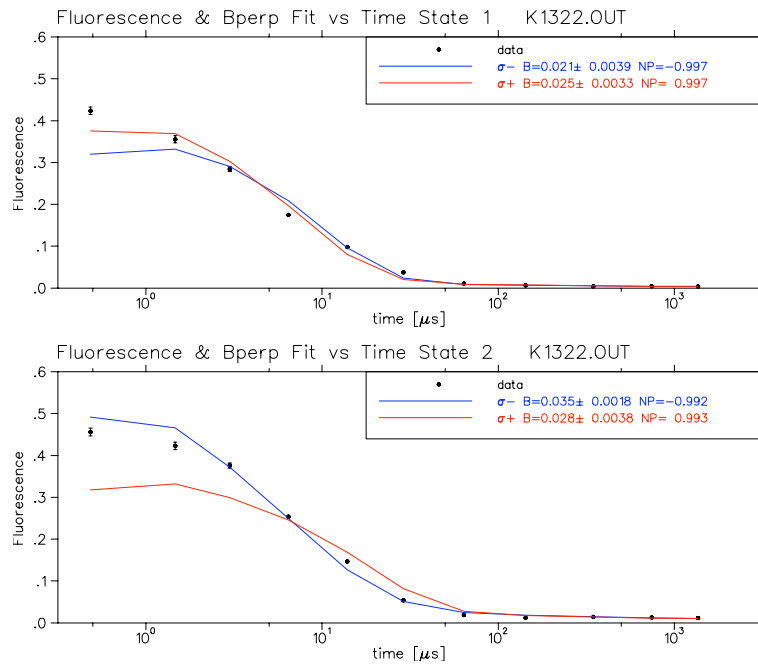
Figure 17: Distinguishing σ^- and σ^+ by fitting data: Laser State A $\leftrightarrow$ LCVR State 1
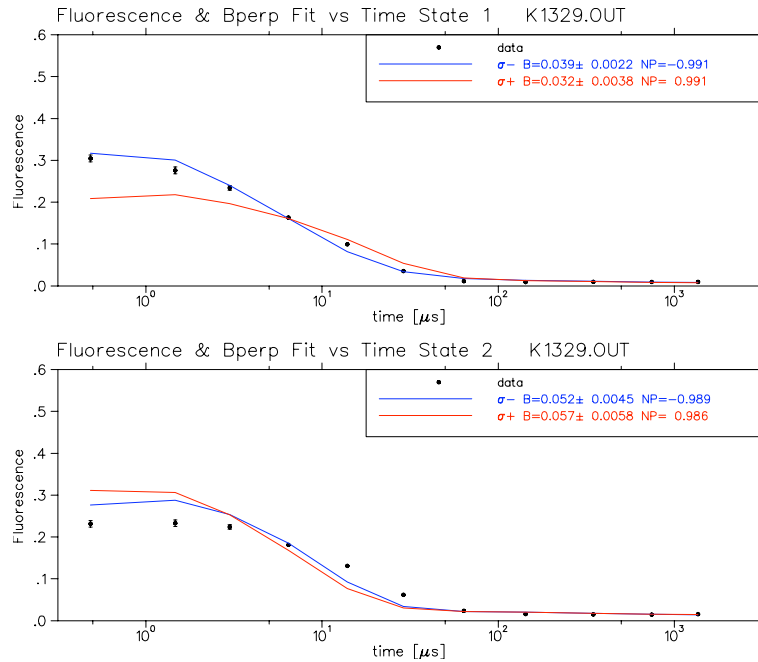
Figure 18: Distinguishing σ^- and σ^+ by fitting data: Laser State B $\leftrightarrow$ LCVR State 1

36

7 Coherent Population Trapping

Coherent population trapping (CPT) is quantum effect that occurs when two states are pumped by two laser beams such that the difference between the frequencies of the laser beams equals the splitting between the two states. In this system, the two initial states are no longer the eigenfunctions. The new eigenfunctions are a bright and a dark state. Atoms in the former can be excited by the laser, atoms in the latter cannot and are therefore "coherently trapped." In the potassium atom, there are three pairs of $S_{\frac{1}{2}}$ states in which CPT can occur. Each pair is formed by two states having equal m_F ($m_F = -1$, $m_F = 0$, and $m_F = +1$) but different F numbers. The pumping laser beam pumps the $F = 2$ state in the pair, and the repumping laser beam pumps the $F = 1$ state. This by design, as optical pumping requires that both states be pumped to the $P_{\frac{1}{2}}$, $F = 2$ state.

None of the CPT pairs include the stretched states having $m_F = +2$ $m_F = -2$, so any coherent population trapping prevents atoms from reaching the stretched states and is undesirable. Fortunately, CPT only occurs if the frequency difference between the two laser beams exactly matches the energy splitting of the two states in the CPT pair. Coherent population trapping can be avoided in two ways. The first is by simply avoiding combinations of pumping and repumping frequencies that differ from each other by one of the CPT frequencies. As will be seen later in this section, the line width of CPT frequencies is on the order of $0.1\ MHz$, so this is not difficult to do. The second method is using counter-propagating beams, because for any atoms having a nonzero velocity on axis with the beams, the Doppler effect shifts the frequencies of the beams so that if one beam creates CPT, the other destroys it. Optical pumping in the MOT is done with counter-propagating beams. However, this second method is not entirely effective, because the atoms that do have zero velocity on axis with the beams can still be coherently trapped.

7.1 CPT Fluorescence Curve Setup

Fluorescence curves were used to find the coherent population trapping frequencies in the system, using the setup shown in Figure 20 and the trap code d7sccpt described in Table 3. The idea is to take a normal fluorescence curve measurement with the first seven scalers with CPT conditions, then detune the repumping beam to destroy the CPT effect while scalers 8 and 9 count, then go back to the previous conditions while scalers 10 and 11 count. When the CPT effect is destroyed, the atoms that were trapped in the dark state should start interacting with the light and a second fluorescence peak will be observed. An example of a CPT curve is shown in Figure 19. The ratio between the second peak or "CPT" peak and the initial fluorescence gives the fraction of atoms that were coherently trapped. As with regular fluorescence curves, the process is repeated many times for both states and their backgrounds, and the backgrounds are subtracted from the fluorescence.

The setup requires two RF sources for the repumping light, one which is set to the CPT frequency (since the frequency of the RF source is the difference between the pumping and
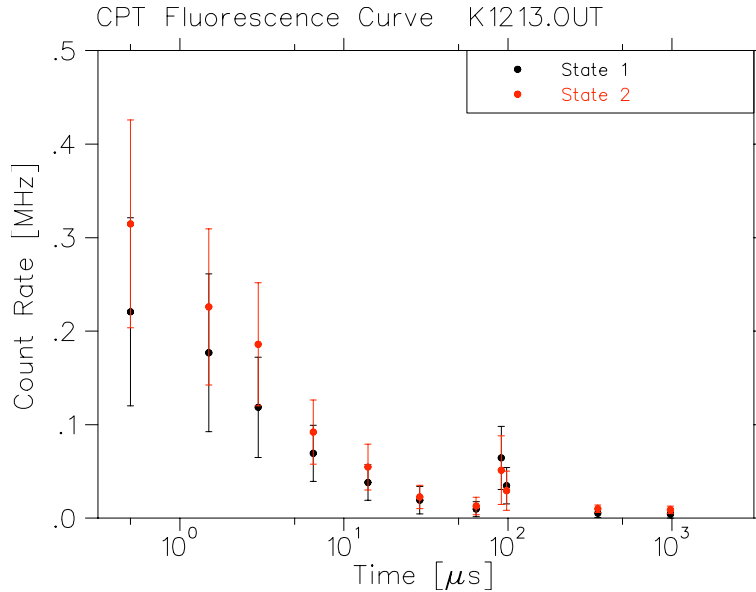
Figure 19: Example CPT fluorescence curve

repumping light), and the other of which is set to a detuning value of 255 MHz which is not expected to create CPT. The CPT RF source is a HP 8640B Signal Generator that can be locked onto frequencies with 1 kHz precision. The detuned RF source is a Mini-Circuits Voltage Controlled Oscillator (ZOS-300). An RF switch (Mini-Circuits ZYSWA-2-50DR) controls which RF source is sent to the laser. A second output of scaler 8 is connected to a gate delay generator (LeCroy 222) that creates a gate equal in length to the sum of the gates on scalers 8 and 9. This gates the RF switch so that the CPT RF source pumps the laser only only while scalers 8 and 9 count. The gate times of scalers 8 and 9 are made much shorter when measuring CPT, which has to be done by hand by adjusting the gate generator potentiometers. The gate widths for this setup are given in Table 7.

Table 7: Scaler gate widths for CPT setup

Scaler	1	2	3	4	5	6	7	8	9	10	11	RF Switch
Gate Width (μs)	1	1	2	5	10	20	50	4	10	500	750	14

Another important part of the setup is blocking one of the counter-propagating laser beams, usually the upward going one. It was observed that with both beams unblocked, some CPT still occured at CPT frequencies, but only a fraction of the amount observed with only one beam.

38
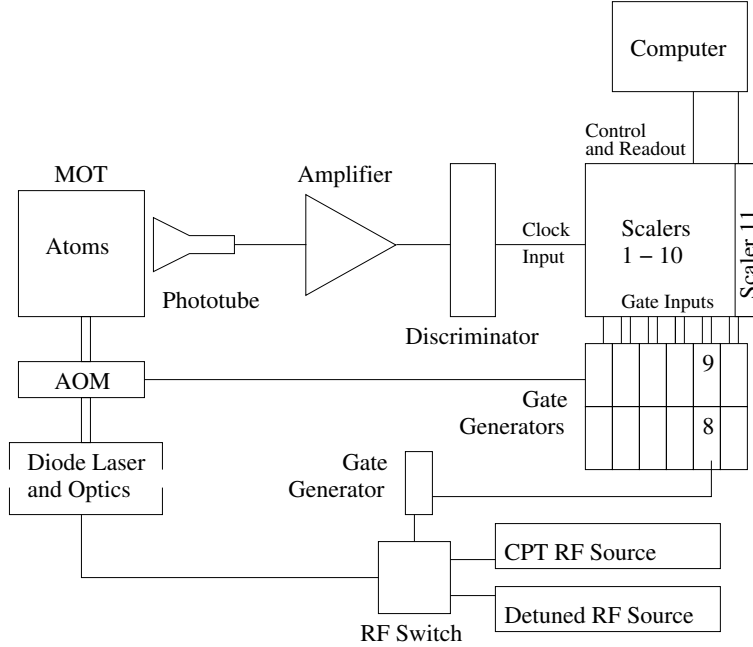
Figure 20: Coherent population trapping fluorescence curve acquisition setup

7.2 CPT Frequency Sweeps with Cyclotron Off and On

The values of the CPT frequencies are dependent on magnetic field in the trap. The value of this field was not known precisely, so the CPT frequencies were also not known. They were found by sweeping over CPT frequency values, and recording the CPT ratio. Doing a frequency sweep requires running the d7sccpt code once for each frequency data point, and changing the frequency on the CPT RF source by hand between each run. The results of six CPT sweeps are shown in Figures 21 and 22. Each data point is a CPT ratio, given by Equation 38, and the errors are statistical counting errors (not RMS errors, which would be very large).

$$CPT^* = \frac{SC8 - SC8B + SC9 - SC9B}{SC1 - SC1B + SC2 - SC2B + SC3 - SC3B} \tag{38}$$

$^*SCX(B) = number\ of\ counts\ in\ scaler\ X\ during\ ``fluorescence"\ (during\ ``background")$

An unweighted Lorentzian fit is shown for each graph, and the center of the Lorentzian was taken to be the CPT frequency for that pair of states. The sweeps in Figure 21 were done in early March before the cyclotron magnet was turned on, while those in Figure 22 were done after the cyclotron was turned on. Because the CPT frequencies depend

on the magnetic field in the trap, the cyclotron's magnetic field in the region of the trap made a measurable difference in these frequencies. Moreover, using the model described in Section 5, the magnetic field in the trap was deduced from the CPT frequencies. Table 8 summarizes the results of the CPT measurements. The errors of the graphs are not included because they are likely underestimates as only counting errors were used for the CPT ratios and the Lorentzian fits are unweighted. A reasonable estimate for the errors would be ± 0.005 MHz for the CPT frequencies and ± 0.02 G for the deduced magnetic fields.

Table 8: CPT frequencies and derived magnetic fields

Cyclotron Magnet Off	
Pair of States m_F	CPT Frequency
-1	251.36 MHz
0	254.07 MHz
$+1$	256.77 MHz
Magnetic Field	1.929 G
Cyclotron Magnet On	
Pair of States m_F	CPT Frequency
-1	251.01 MHz
0	254.09 MHz
$+1$	256.14 MHz
Magnetic Field	2.1914 G

7.3 CPT Parameter Sweeps

An attempt was made to use CPT sweeps to optimize the current in the trim coils using d7cptswp. This procedure is similar to parameter sweeps using tail to peak discussed in Section 4, but instead of taking tail to peak as an indicator of nuclear polarization and therefore of field-laser alignment, the CPT ratio is taken to be an indicator of the alignment. Since CPT occurs between states of equal m_F, and perpendicular fields mix states of different m_F, the CPT ratio should decrease when perpendicular fields are present. CPT sweep of the B_{X2} and B_{Z2} coils were carried out at the $m_F = 0$ CPT frequency. The CPT sweeps were found to be considerably less sensitive to the field from the B_{Z2} trim coils than the tail to peak sweeps, and were completely insensitive to the field from the B_{X2} coils. It is possible that CPT in the other two states, $m_F = -1$ or $m_F = +1$ is more sensitive to perpendicular fields, particularly because those energy levels and therefore their CPT frequencies depend linearly on field, while the $m_F = 0$ states and therefore their
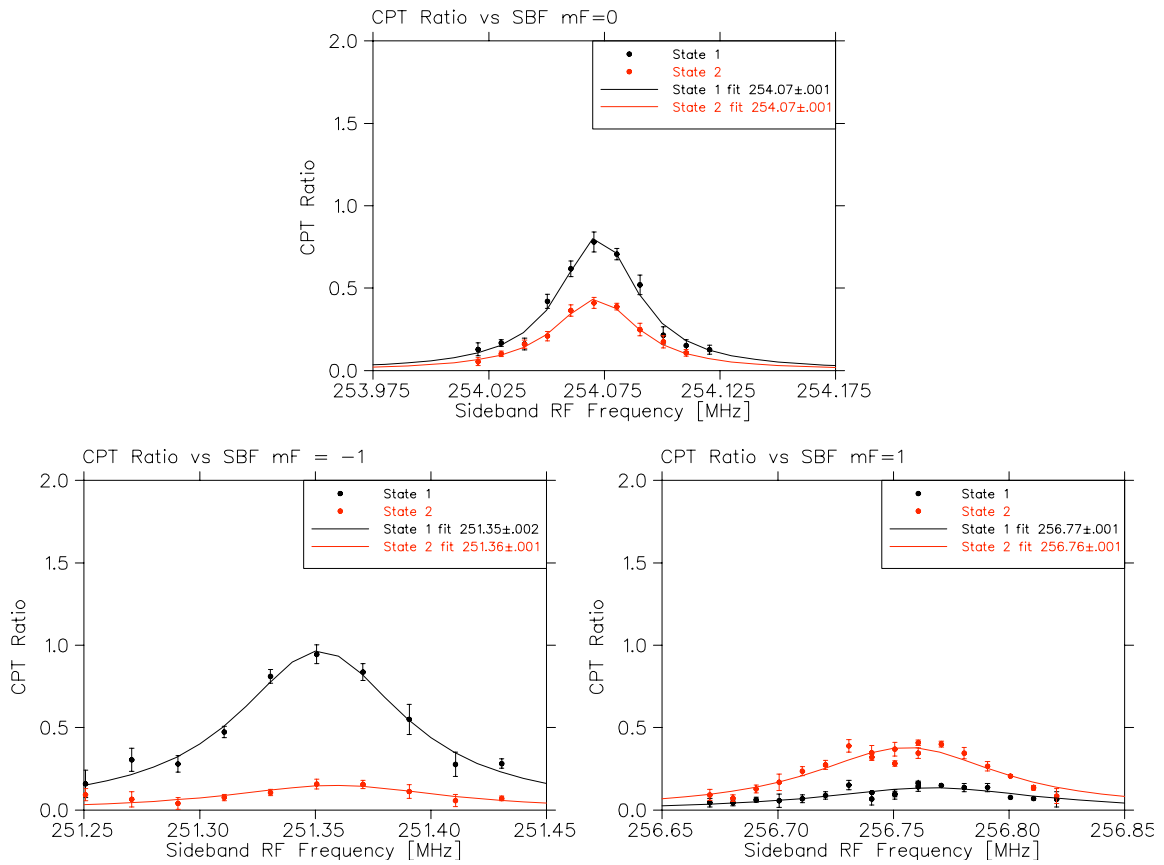
Figure 21: CPT sweeps with cyclotron off
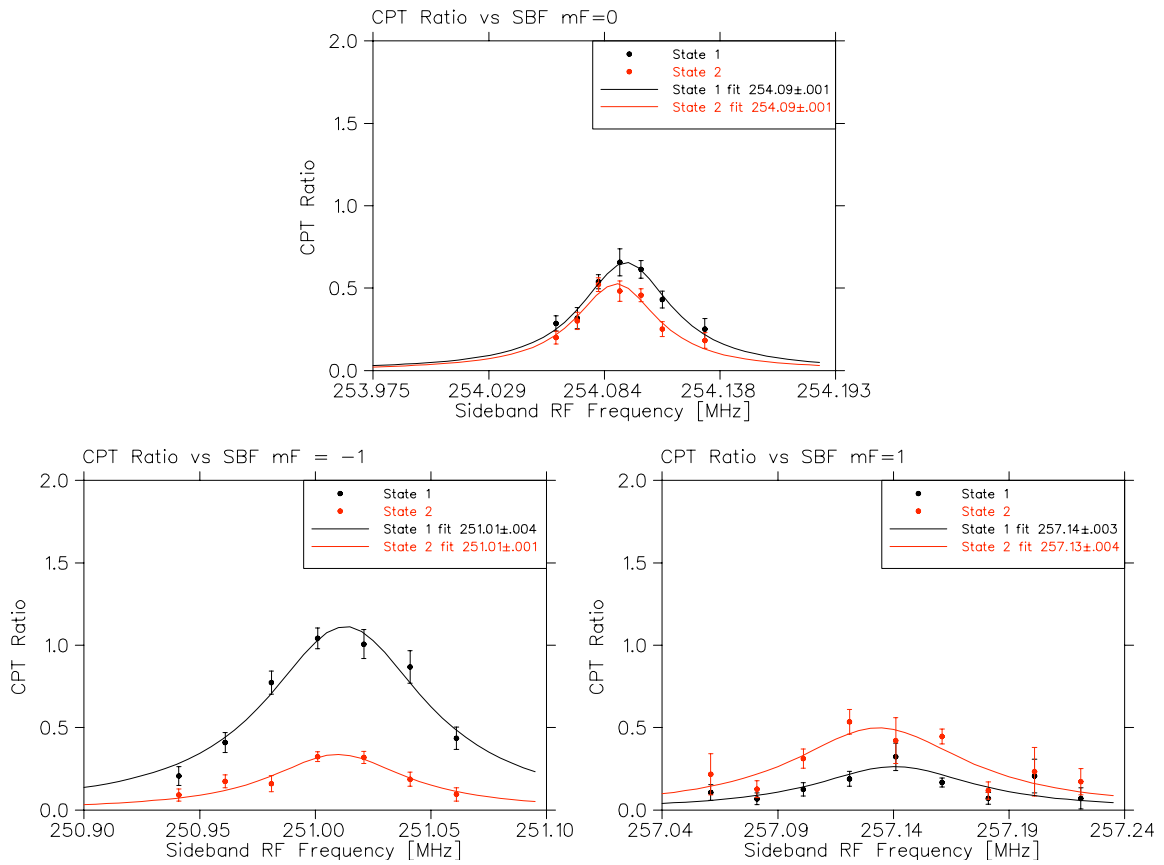
Figure 22: CPT sweeps with cyclotron on

CPT frequency vary only quadratically with field. CPT sweeps using the other two states have not yet been attempted.
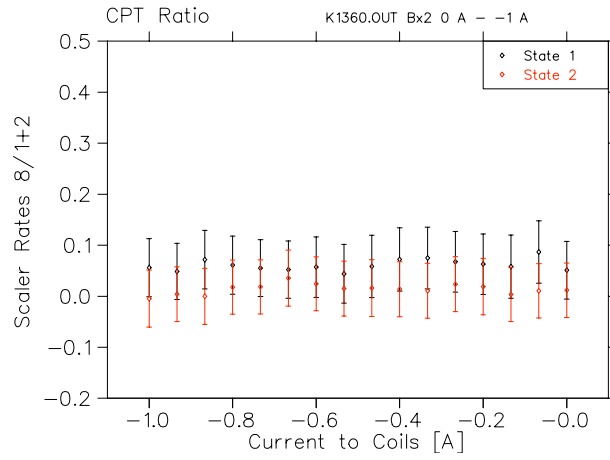
Figure 23: CPT B_{X2} sweep
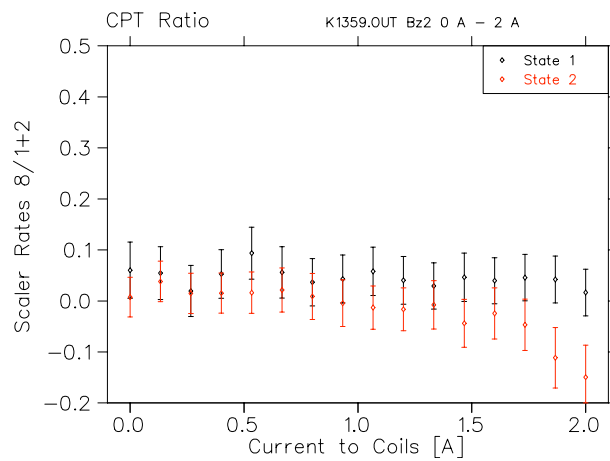
Figure 24: CPT B_{Z2} sweep

8   Additional Work

8.1   Power in Optical Pumping Beams

A difference in laser power from one polarization state to another could cause differences in nuclear polarization in the two states, which would be a problem for symmetry experiments. As can be seen from any of the graphs in the report, State 1 fluorescence curves are fairly consistently lower than those for State 2. It was hypothesized that perhaps the difference was a result of different power in the optical pumping light in the two LCVR states. To determine if this was the case, a photodiode (Newport 818-SL) was placed between the quarter wave plate and the chamber on the downward going beam arm, and the output was recorded on an oscilloscope. This was done for both LCVR states and for both beams (for the upward beam, the photodiode was turned around). The photodiode was not optimally positioned, so the measurements only give an indication of relative beam intensities.

Table 9 shows the power in each state for both beams, in units of mV measured on the oscilloscope, and errors estimated for cursor readings on the oscilloscope. While there is a significant difference in intensity of the two beams, there differences between the two LCVR states for either beam are within the error bars.

Table 9: Relative Power in Optical Pumping Beams for Both States

Beam	LCVR State	Power Measurement
Downward	1	259 ± 8
Upward	1	202 ± 8
Downward	2	264 ± 8
Upward	2	210 ± 8

The maximum absolute power of the downward beam was also determined to be 0.3735 mW/cm^2. The photodiode, having a 1.3 cm active diameter measured the power as 0.34 mW. Assuming a beam intensity profile having a gaussian profile with I_{max}/e^2 at 0.9 cm, and integrating over the area of the photodiode, I_{max} was found to be 0.3735 mW/cm^2. This is taken to be the power of the each of the beams seen by the atoms, as they are in a 3mm cloud at the center of the beam, so the power can roughly be assumed to be constant and equal to I_{max} over the atom cloud.

8.2 Background in Phototube as a Function of Beam Aperture

For fluorescence measurements, it would be desireable to minimize the background in the phototube from the optical pumping light without significantly decreasing the diameter and therefore the power of the beam. A test was done to determine if the background rates in the phototube very linearly or otherwise with beam diameter. The upward going beam was blocked, and a variable aperture was placed between the downward going beam and the chamber. The average counts in the phototube were measured as the size of the aperture was changed, and the results are shown in Figure 25. The phototube signals were amplified then passed through a discriminator, then to the Triumf Visual Scaler. Due to varying mismatch between AC MOT/optical pumping cycles and the sampling window of the scaler, the count rate oscillated, so both maximum and minimum count were recorded. The trend is linear for large apertures, which is the region corresponding to realistic beam diameters. This shows that it is not possible to minimize background without significantly reducing the beam diameter.
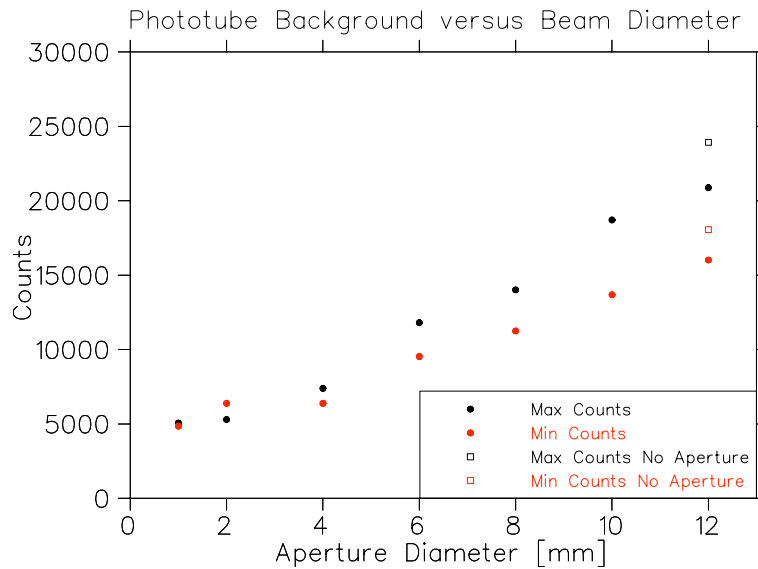
Figure 25: Phototube background as a function of beam diameter

9   Conclusion and Recommendations

The fluorescence curve acquisition system has been useful in measuring the trap field, minimizing perpendicular fields, and identifying CPT frequencies. There iremains work to be done to minimize errors in the fluorescence curves, and in determining which state corresponds to which circular polarization. The following recommendations are made for continuing the work described in this report:

- Continue work to understand the errors associated with S_3 measurement assumptions

- Develop a method to correct fluorescence measurements for the number of atoms in the trap using the CCD camera image

- Develop a method to correct fluorescence measurements for laser power drift by sampling the optical pumping light

- Remeasure the B_{Z2} trim coil sweep with the cyclotron magnet on to obtain a more reliable minimum value

- Determine which σ corresponds to which LCVR state using beta or recoil distributions relative to the magnetic field

- Try doing CPT parameter sweeps with the $m_F = -1$ or $m_F = +1$ states

References

[1] W. H. McMaster, "Polarization and the Stokes Parameters" Am. J. Phys., vol. 22, no. 6, pp. 351-362 Sep 1954

[2] M. Groves, *Optical Pumping Beam Polarisation and its Effects on ^{41}K Fluorescence,* TRINAT Co-op Report, May 2001.

[3] B.H. Billings, E.H. Land, "A Comparative Survey of Some Possible Systems of Polarized Headlights," J. Opt. Soc. Am., vol. 38, no. 10, pp. 819-829, Oct 1948

[4] Meadowlark Optics. (Accessed 2013, April 25) *Liquid Crystal Variable Retarders* [Online] Available: `http://www.meadowlark.com/liquid_crystal.php?pg=liquid`

[5] S. Falke, E. Tiemann, C. Lisdat, H. Schnatz, G. Grosche, "Transition frequencies of the D lines of ^{39}K, ^{40}K, and ^{41}K measured with a femtosecond laser frequency comb." Phys. Rev. A., vol. 74, no. 032503, pp. 1-9 Sep 2006

[6] E. Arimondo, M.Inguscio, P.Violino, "Experimental determinations of the hyperfine structure in alkali atoms" Rev. Mod. Phys., vol. 49, no. 1, Jan 1977

[7] A. Corney, 'The Hyperfine Structure of Atoms" in emphAtomic and Laser Spectroscopy New York, Oxford Univ. Press, 1979, ch. 18, pp.661-673